creative commons

COMMONS DEED

저작자표시-비영리-변경금지 2.0 대한민국

이용자는 아래의 조건을 따르는 경우에 한하여 자유롭게

- 이 저작물을 복제, 배포, 전송, 전시, 공연 및 방송할 수 있습니다.

다음과 같은 조건을 따라야 합니다:

저작자표시. 귀하는 원저작자를 표시하여야 합니다.

비영리. 귀하는 이 저작물을 영리 목적으로 이용할 수 없습니다.

변경금지. 귀하는 이 저작물을 개작, 변형 또는 가공할 수 없습니다.

- 귀하는, 이 저작물의 재이용이나 배포의 경우, 이 저작물에 적용된 이용허락조건을 명확하게 나타내어야 합니다.
- 저작권자로부터 별도의 허가를 받으면 이러한 조건들은 적용되지 않습니다.

저작권법에 따른 이용자의 권리는 위의 내용에 의하여 영향을 받지 않습니다.

이것은 이용허락규약(Legal Code)을 이해하기 쉽게 요약한 것입니다.

Disclaimer

dCollection

공학석사 학위논문

Numerical study on diffraction problem for a truncated cylinder with dual dampers

이중 감쇠판이 부착된 절단 실린더 주위의 파 회절 문제에 대한 수치 연구

2023년 2월

서울대학교 대학원

조선해양공학과

송 진 호

이중 감쇠판이 부착된 절단 실린더 주위의 파 회절 문제에 대한 수치 연구

Numerical study on diffraction problem for a truncated cylinder with dual dampers

지도 교수 남 보 우

이 논문을 공학석사 학위논문으로 제출함
2023년 1월

서울대학교 대학원
공과대학 조선해양공학과
송 진 호

송진호의 공학석사 학위논문을 인준함
2023년 1월

위 원 장 _____ 김 용 환 _____

부 위 원 장 _____ 남 보 우 _____

위 원 _____ 김 도 균 _____

ABSTRACT

In the last decades, offshore wind energy industries have moved to deep sea area, since 80% of the offshore wind resources are located in deep water region (over 60 meters). As a result, various floating offshore wind turbine (FOWT) structures based on the semi-submersible, TLP or spar platforms have been widely proposed. However, accompanied with abundant wind resources, harsher environmental loads in deep sea area may also cause damage to offshore structures. In general, the semi-submersible platform of FOWT are mainly composed of large truncated circular columns which tend to generate significant diffraction effects under the incident waves. These diffraction effects are usually associated with significant rapid amplification of local free-surface elevation surrounding these cylindrical structures. Therefore, single dampers with arbitrary shapes are commonly attached at the bottom of FOWT to improve the motion performance of the FOWT system.

The present research aims to investigate the effects of the separating distance, the porosity and the thickness of the damping plate on wave run-up around the truncated cylinder with dual dampers under the regular wave conditions. The target model is an offset column of OC4-DeepCWind FOWT. To evaluate the three-dimensional (3-D) wave run-up around the truncated cylinder with dual dampers in a finite water depth, a matched eigen-function expansion method (MEEM) based on linear potential theory was developed. In this study, fluid around the truncated cylinder was divided into multiple regions based on different boundary conditions. The velocity potential in each region is analytically derived by using the Helmhotz Equation and eigen-function expansion. Darcy's law is applied to satisfy the boundary condition on the porous damping plate. The velocity and pressure of fluid across the adjacent

sub-regions should satisfy the continuous conditions (mass conservation) on the boundary. Finally, the unknown complex coefficients matrix could be derived and solved by using the matching conditions along the boundaries of regions.

The present MEEM solutions for the truncated cylinder with various types of damping plate are validated by comparing with BEM solutions. Furthermore, with regard to the other simple porous structures such as horizontal porous membrane, the complex wave number, wave run-up and hydrodynamic loads are also compared to previous computational results. The results of present study clearly indicate that compared with the impermeable damping plate, porous damper could significantly reduce the heave wave exciting force and wave run-up around the truncated cylinder. Impermeable dual damping plates with large separating distance could cause significant wave run-up and hydrodynamic loads acting on truncated cylinder due to the shallow water effect in the local flow. It is expected that present porous dual damping plate model can be applied to the offshore structures such like FOWT.

Keyword: dual damping plate (DDP), diffraction, porous heave damper, wave run-up, linear potential theory, truncated cylinder

학번: 2020-26705

Content

ABSTRACT **1**

Content **1**

1. Introduction **1**

1.1 Research background 1

1.2 Research objectives 6

2. Numerical Method **8**

2.1 Mathematical Formulation 8

2.2 Analytical solutions in sub-regions 15

2.3 Computation of unknown coefficients 23

2.4 Computations of wave run-up and hydrodynamic forces 26

3. Validation of Numerical Method **30**

3.1 Case I: Truncated cylinder with impermeable damping plate 30

3.2 Case II: Permeable structure 37

4. Results and Discussion **45**

4.1 Effect of Separation Distance 45

4.2 Effect of porosity 52

4.3 Effect of thickness 63

5. Conclusions **68**

Reference **70**

List of Table

Table. 2.1 Geometric properties of truncated cylinder and dampers 9

Table. 2.2 Convergence study of normalized wave run-up η/A around the truncated cylinder with dual dampers for ka=0.2 29

List of Figure

Fig. 2.1 Target truncated cylinder model with three types of dampers 8

Fig. 2.2 Schematic diagram of truncated cylinder with dual dampers 10

Fig. 2.3 Schematic of dual damping plate w.r.t different porous effect parameter 19

Fig. 2.4 Behavior of roots for the porous damping pate dispersion relationship using Newton's method.....22

Fig. 2.5 Position of wave probes on the truncated cylinder 27

Fig. 3.1 Panel model of truncated cylinder with three types of damping plate 30

Fig. 3.2 Comparison of dimensionless wave run-up around truncated cylinder with single thin damper between present MEEM & BEM solution.....33

Fig. 3.3 Comparison of dimensionless wave run-up around truncated cylinder with dual thin dampers between present MEEM & BEM solution.....35

Fig. 3.4 Comparison of dimensionless wave run-up around truncated cylinder with single thick damper between present MEEM & BEM solution....36

Fig. 3.5 Schematic figure for three special porous structures: (a) single horizontal porous membrane; (b) porous truncated cylinder with inner porous plate; (c) porous truncated cylinder 38

Fig. 3.6 Validation for the complex wave numbers for first five modes: (a) $k_0h = 2.0$; (b) $k_0h = 4.0$ (k_0: wave number) 39

Fig. 3.7 Validation for the wave elevation around a porous horizontal membrane: (a) Wave Probe 1 (0°); (b) Wave Probe 3 (90°); (c) Wave Probe 5 (180°) 41

Fig. 3.8 Validation for the surge and heave wave exciting force acting on porous structure: (a) porous truncated cylinder; (b) porous truncated cylinder with

inner porous plate.....43
Fig. 4.1 Comparison of dimensionless wave run-up around truncated cylinder with different normalized separating distance d/D between dual dampers 46
Fig. 4.2 Distribution of wave amplitude around the truncated cylinder with impermeable dual damping plate ($d/D = 0.3$) with different scattering parameters: (a) *ka*=0.2; (b) *ka*=1 47
Fig. 4.3 Distribution of wave amplitude around the truncated cylinder with impermeable dual damping plate ($d/D = 0.6$) with different scattering parameters: (a) ka=0.2; (b) ka=1.....48
Fig. 4.4 Comparison of dimensionless wave exciting forces around truncated cylinder with different separating distance d/D between dual dampers: (a) surge exciting force; (b) heave exciting force.....50
Fig. 4.5 Comparison of dimensionless wave run-up around truncated cylinder with different b_0 for upper damper 53
Fig. 4.6 Distribution of wave amplitude around the truncated cylinder with porous dual damping plate ($b_0 = 0.001, b_1/h = 0.025$) with different scattering parameters: (a) *ka*=0.2; (b) *ka*=1 54
Fig. 4.7 Distribution of wave amplitude around the truncated cylinder with porous dual damping plate ($b_0 = 23, b_1/h = 0.025$) with different scattering parameters: (a) *ka*=0.2; (b) *ka*=1 55
Fig. 4.8 Comparison of dimensionless wave exciting forces around truncated cylinder with different b_0 for upper damper ($b_1/h = 0.025$): (a) surge exciting force; (b) heave exciting force.....57
Fig. 4.9 Comparison of dimensionless wave run-up around truncated cylinder with different b_0 for upper damper ($b_1/h = 0.05$).....60
Fig. 4.10 Distribution of wave amplitude around the truncated cylinder with

porous dual damping plate ($ka = 0.6, b_1/h = 0.05$) with various porosities: (a) b_0=0.001; (b) b_0=23.....60
Fig. 4.11 Comparison of dimensionless wave run-up around truncated cylinder with different normalized thickness T/D of single thick damper 64
Fig. 4.12 Schematic of truncated cylinder with single thick damper and dual thin damping plates 65
Fig. 4.13 Comparison of dimensionless wave run-up around truncated cylinder with dual damping plate and single thick damper.....66

1. Introduction

1.1 Research background

In the last decades, the production of offshore wind energy has increased rapidly, and the installed capacity of the offshore wind power industry reached 5519MW by 2020 **(Floating offshore wind energy, 2018)**. Approximately 80% of the offshore wind resources are located in deep water region (over 60 meters), as developers prefer to use the largest offshore wind turbine available for a given project which reduces balance-of-system costs on a per-kilowatt basis **(Walter et al., 2021)**. In the deep water region, floating offshore wind turbines (FOWT) based on semi-submersible, TLP or spar platforms have been more widely utilized than fixed offshore wind turbines.

According to a report from InfoLink Consulting **(InfoLink, 2021)**, the installed capacity as well as the amount of semi-submersible type wind farms have increased rapidly since 2021. In addition, the number of the semi-submersible type wind farms is expected to exceed the number of spar type wind farms after 2022. This is mainly because the semi-submersible foundations are much easier to install and tow due to the low draught comparing with spar foundations.

Along with the plentiful wind resources in the deep sea, harsher environmental conditions may cause damage to offshore structures. Generally, a semi-submersible platform of FOWT consists of several vertical columns, which have the shape of a circular cylinder or polygonal cylinder. To improve the motion performance of FOWT, various types of dampers are often attached to the bottom of the supporting columns. The FOWT structures using dampers

include WindFloat **(Roddier et al., 2010)**, OC4-DeepCWind **(Robertson et al., 2014)**, Tri-floater **(Lefebvre et al., 2012)** and Dutch Tri-floater **(Huijs et al., 2014)**. These cylindrical columns tend to create substantial diffraction and radiation effects under incident waves. These diffraction effects are usually associated with significant rapid amplification of local free-surface elevation around the cylindrical structures.

To address wave diffraction problem due to the cylinder-damper structure, it is necessary to understand the fundamental characteristics of wave run-up around a cylinder in waves. Many researchers have conducted experimental studies and CFD simulations about the wave diffraction problem of a circular cylinder. **Mohapatra et al. (2020)** calculated wave run-up and wave impact acting on a truncated cylinder by developing a new Boussinesq equations (Bes) model. By comparing the results with CFD and experimental data, they found that the trends of wave amplitude around the cylinder could be captured efficiently. **Mohseni et al. (2018)** conducted a CFD simulation by using OpenFOAM to examine the physics of wave scattering and wave run-up around a truncated cylinder with the consideration of high steep waves. **Thomas et al. (2004)** conducted a model test to discuss wave run-up on a fixed truncated cylinder with harmonic analysis in monochromatic progressive waves. **Lee et al. (2021)** applied the commercial CFD code STAR-CCM+ to study the nonlinear wave run-up around a truncated cylinder under various wave period and slope conditions. **Cha et al. (2016)** measured wave run-up height and depression depth around offshore cylindrical structures with various wave periods based on CFD simulations. **Cao et al. (2015)** presented a numerical investigation of solitary wave run-up around a circular cylinder by using a viscous numerical wave tank (NWT). **Nam et al. (2008)** carried out a benchmark experimental study for wave run-up around a truncated cylinder in a finite water depth and validated the results against both the CFD and potential solutions. **Kim et al. (2011)** applied an efficient NWT model for CFD

simulations based on the ALE Finite-Element method (FEM) to estimate wave run-up of a truncated vertical cylinder exposed to long nonlinear regular waves.

As noted, heave dampers have been widely used in conjunction with spar-type offshore structures to reduce heave and pitch motion by increasing the added mass and damping thereby changing the resonance period. **Thiagaranjan et al. (2002)** investigated the possibility of adding a heave plate at the base of a production spar installed in West African offshore. Through CFD simulations and experiments, they suggested that the damper extension should be at least four times the typical heave amplitude to maximize the drag effect. **Tao et al. (2004)** proposed a spar with single damping plate to investigate the effect of damper shape on viscous damping and heave motion response based on CFD simulations. **Sudhakar et al. (2011)** conducted both the experiments and potential calculations on a floating spar model with a heave damping plate. By comparing various geometric parameters, an optimum heave response was achieved when the heave plate diameter was 20% to 30% larger than the diameter of the spar. **Seebai and Sundaravadivelu (2013)** performed a model test on a spar-type FOWT, taking into consideration both circular and square heave damping plates. It was observed that the circular heave damper was more effective in reducing the heave motion response of the FOWT. **Subbulakshmi et al. (2016)** compared the effect of a single heave plate and dual heave plates on the heave motion of a spar based on CFD simulations and model tests. They reported that the heave motion of the cylinder decreased with larger separating distance of dual damping plates. **Rao et al. (2021)** proposed both numerical and experimental analysis to evaluate the heave damping force of a classic spar with dual dampers by conducting the free decay tests in calm water.

Porous structures in ocean engineering have been widely applied to various

types of breakwaters in coastal areas, as they are capable of reducing the hydrodynamic loads and wave run-up. Consequently, diffraction problems due to porous media draw the attention of researchers, **Zhao et al. (2012)** conducted model tests to evaluate the efficiency of wave dissipation among a porous cylinder array. They found an optimum array by properly adjusting the number, spacing and draft of cylinders. Subsequent investigations of wave diffraction from an array of bottom-mounted porous cylinders have been conducted by other scholars (**Williams et al., 2000; Li et al., 2004; Sankarbabu et al., 2007; Park et al., 2007**). **Feichtner et al. (2021)** then applied a porous-media approach in CFD simulation. With the approximation of homogeneous pressure-drop in all directions of a porous cylinder, wave forces agreed well with the experimental results. **Mackay et al. (2021)** further employed a boundary element method (BEM) to measure the wave exciting forces and radiation forces on a cylinder with a porous sidewall. They found that the surge damping forces due to the dissipation of energy through the porous surface is significantly increased. **George et al. (2022)** investigated the effect of porosity of a heave disk on the damping force based on CFD simulations. It was reported that the maximum damping could be achieved with porosities of 0.049 and 0.11 for various Keulegan-Carpenter (KC) numbers.

The earliest works pertaining to the wave-body diffraction problem around a truncated cylinder in deep water was given by **Havelock et al. (1940). Omer and Hall (1949)** and **MacCamy and Fuchs (1954)** then extended Havelock's work into shallow water and arbitrary water depth respectively. In the past decades, many researchers have been interested in the interaction between the submerged porous structure and waves by using analytical solutions. **Chwang and Wu (1994)** first proposed a benchmark study on wave run-up around a fixed horizontal porous disk by employing the method of matched eigen-

function expansion based on linear potential theory. They assumed the thickness of the disk to be zero, and thus Darcy's law was applied as the vertical boundary condition on the horizontal plate. His results implied that the wave elevations around the disk could be significantly reduced with the consideration of the porosity. Subsequently, **Cho and Kim (2000)** investigated the effect of porosity on the wave-blocking efficiency of a horizontal flexible membrane by utilizing a two-dimensional (2D) analytical method. They reported that the porous horizontal membrane could significantly increase energy dissipation when the submergence depth was small. **Bao et al. (2009)** calculated the wave forces and radiation forces on a porous circular cylinder with a horizontal porous plate fixed inside. By comparing the results between analytical solutions and model tests, they found that the porous damping induced by the pore was much larger than the potential damping. **Zhao et al. (2011)** investigated **s**urge, heave and pitch wave exciting forces (moment) acting on a porous truncated cylinder analytically and significant reduction of forces was observed with the application of a porous sidewall. Additionally, to find the hybrid structure with better hydrodynamic performance, many researchers (**Yu et al., 1995; Liu et al., 2007; Mandal et al., 2013; Park et al., 2015; Ning et al., 2017; Sarkar et al., 2020; Wang et al., 2021)** have also conducted analytical studies to evaluate the attenuating effect of porous structure on wave force and wave run-up.

1.2 Research objectives

The main objective of this study is to investigate the interaction between water waves and a truncated circular cylinder with various types of heave dampers. The target model is an offset column of OC4-DeepCWind FOWT. To evaluate the three-dimensional (3-D) wave run-up around a truncated cylinder in a finite water depth, an analytical solution based on the matched eigen-function expansion method was developed based on the Airy (linear) wave theory.

In this study, the fluid domain surrounding the truncated cylinder was divided into several regions based on different boundary conditions. The velocity potential in each region was analytically derived by using the Helmhotz Equation and eigen-function expansion. The boundary condition on the porous damper was defined by applying Darcy's law under the assumption of fine pores and negligible wall thickness. The velocity and pressure of the fluid across the adjacent sub-regions satisfied the continuous conditions (mass conservation) at the boundary. Finally, the analytical solutions in the different regions were found by employing the matching conditions along the boundaries of the regions.

The present MEEM solutions are validated by direct comparison with computational results of other porous structures, such as horizontal porous membrane. Furthermore, wave elevations around a truncated cylinder with different types of impermeable heave damping plate are also compared to BEM solutions.

To investigate the effect of damping plates on wave run-up around the truncated cylinder, a series of parametric studies have been conducted. The effects of various wave parameters (wave frequency) and the geometric parameters of the damper (separating distance, thickness and porosity) on wave

run-up around the truncated cylinder have been illustrated. In addition, the hydrodynamic loads acting on the entire cylinder have been analyzed with regard to the porous damping plate.

2. Numerical Method

2.1 Mathematical Formulation

In this study, three models of the truncated cylinder with various heave damping plates are considered as shown in Fig.2.1. The first two models are truncated cylinders with a thin and thick single damper. Regarding the truncated cylinder with dual damping plate in the last figure, an impermeable damping plate is assumed to be located at the bottom as well as a porous damping plate in the middle. The dimensions of the cylinder and the damper used in this study are given in Table 2.1, where the cylinder with thick damper is identical to the offset column of OC4-DeepCWind FOWT.

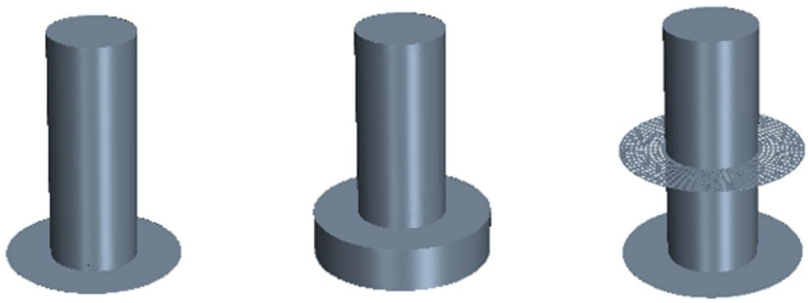

Fig. 2.1 Target truncated cylinder model with three types of dampers

The schematic of wave diffraction for a truncated circular cylinder with dual damping plates is illustrated in Fig. 2.2. Symbols a_1, a_2, b_1, b_2 and h represent the radius of the truncated cylinder, the radius of damping plate, the draft of upper porous damper, the draft of lower damper and the water depth, respectively. Since it is a 3D diffraction problem, a cylindrical polar coordinate system (r; θ, z) is established with the origin located at the center of the truncated cylinder

on the undisturbed water level.

Table 2.1 Main dimensions of truncated cylinder and dampers

Properties	Dimension
Radius of cylinder [m]	6
Draft [m]	20
Water depth [m]	200
Radius of damper [m]	12
Thickness of damper [m]	6
Separating distance of dual damper [m]	6

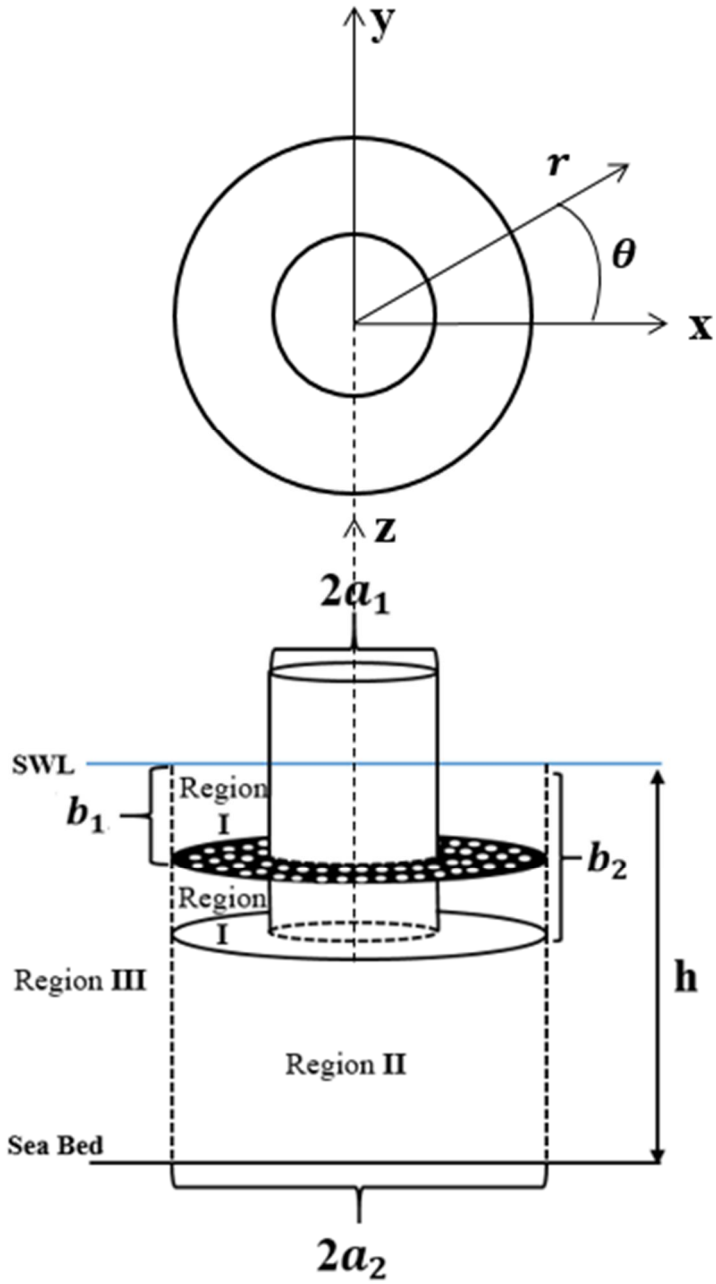

Figure 2.2 Schematic diagram of truncated cylinder with dual dampers

By adopting linear water wave theory, the fluid can be described in terms of velocity potential $\Phi(r,\theta,z,t) = Re\left[\phi(r,\theta,z)e^{-i\omega t}\right]$ based on the assumption of an incompressible and inviscid fluid with irrotational motion. Here $\phi(r,\theta,z)$ denotes the spatial velocity potential of the fluid and ω represents the angular frequency of the incident wave. Since a frequency-domain linear analysis is performed in this study, the time-dependent term $e^{-i\omega t}$ is removed from all the dynamic variables for convenience hereafter.

As illustrated in Fig. 2.2., following **Yeung et al. (1981), Bhatta et al. (2003)** and **Finnegan et al. (2011),** the fluid domain around the truncated cylinder is divided into three regions: an outer region (Region III, $-h \le z \le 0, r \ge a_2$), an inner region adjacent to the cylinder (Region I, $-b_2 \le z \le 0, a_2 \ge r \ge a_1$) and another region below the cylinder (Region II, $-h \le z \le b_2, a_2 \ge r \ge 0$). The velocity potential in each region (Region I, Region II and Region III) is represented by $\phi_j, j = 1,2,3$ which satisfy the Laplace equation, namely

$$\nabla^2\phi_j = 0 \qquad \text{for} \quad j = 1,2,3 \tag{2.1}$$

The kinematic free surface boundary condition (Eq. 2.2-a) and dynamic free surface boundary condition (Eq. 2.2-b) can be combined into a single boundary condition (Eq. 2.2-c) exclusively for the velocity potential (**Linton et al., 2001**).

$$\frac{\partial\eta}{\partial t} = \frac{\partial\phi}{\partial z} \qquad \text{on} \quad z = 0 \tag{2.2-a}$$

$$\frac{\partial\phi}{\partial t} + g\eta = 0 \qquad \text{on} \quad z = 0 \tag{2.2-b}$$

$$\frac{\partial\phi_j}{\partial z} = \nu\phi_j \qquad \text{on} \quad z = 0,\ j = 1,3 \tag{2.2-c}$$

where g denotes the acceleration of gravity and $\nu = \omega^2/g$. The velocity potentials in various regions also satisfy appropriate boundary conditions. In Region III, the velocity potential ϕ_3 satisfies the linear free surface boundary condition (Eq. 2.3-a) and sea bed boundary condition (Eq. 2.3-b). Since Region III is the exterior region extending to infinity, the velocity potential in this region also satisfies the Sommerfeld far-field radiation condition (Eq. 2.3-c) (**Atkinson et al., 1949; Zienkiewicz et al., 1979**):

$$\frac{\partial \phi_3}{\partial z} = \nu \phi_3 \qquad \text{on} \quad z = 0,\ r \geq a_2 \tag{2.3-a}$$

$$\frac{\partial \phi_3}{\partial z} = 0 \qquad \text{on} \quad z = -h,\ r \geq a_2 \tag{2.3-b}$$

$$\lim_{r \to \infty} \left[\sqrt{r} \left(\frac{\partial \phi_d}{\partial r} - ik\phi_d \right) \right] = 0 \qquad \text{on} \quad z = -h,\ r \geq a_2 \tag{2.3-c}$$

where, k denotes the wave number. In Region II, the fluid is below the truncated cylinder, and the velocity potential ϕ_2 satisfies the boundary condition on the sea bed and cylinder bottom, namely

$$\frac{\partial \phi_2}{\partial z} = 0 \qquad \text{on} \quad z = -h, \quad r \leq a_2 \tag{2.4-a}$$

$$\frac{\partial \phi_2}{\partial z} = 0 \qquad \text{on} \quad z = -b_2,\ r \leq a_2 \tag{2.4-b}$$

Region I is the inner region surrounding the truncated cylinder, for which the velocity potential ϕ_1 in this region satisfies the linear free surface boundary condition (Eq. 2.5-a), the body boundary condition (Eq. 2.5-b) on the

impermeable lower damping plate, the porous wall boundary condition (Eq. 2.5-c) on the permeable upper damper. In addition, the velocity potential in inner region also satisfies the boundary condition (Eq. 2.5-d) on the sidewall of the truncated cylinder in the horizontal direction.

$$\frac{\partial \phi_1}{\partial z} = \nu \phi_1 \qquad \text{on} \quad z = 0, \quad a_2 \geq r \geq a_1 \tag{2.5-a}$$

$$\frac{\partial \phi_1}{\partial z} = 0 \qquad \text{on} \quad z = -b_2, \quad a_2 \geq r \geq a_1 \tag{2.5-b}$$

$$\left.\frac{\partial \phi_1}{\partial z}\right|_{z=-b_1^+} = \left.\frac{\partial \phi_1}{\partial z}\right|_{z=-b_1^-} = i\sigma_0\left(\left.\phi_1\right|_{z=-b_1^+} - \left.\phi_1\right|_{z=-b_1^-}\right) \qquad \text{for} \quad z=-b_1, \quad a_2 \geq r \geq a_1 \tag{2.5-c}$$

$$\frac{\partial \phi_1}{\partial r} = 0 \qquad \text{for} \quad 0 \geq z \geq -b_2, \quad r = a_1 \tag{2.5-d}$$

With respect to the porous boundary condition (Eq. 2.5-c), b_1^+ and b_1^- represent the top and bottom sides of the upper damping plate, respectively, as illustrated in Fig. 2.2. Symbol σ_0 denotes the porous effect parameter of the permeable upper damping plate, which is defined as $\sigma_0 = \rho l_0 \omega / \mu$, where ρ represents the density and μ is the dynamic viscosity of water. l_0 indicates the porous coefficient with the dimension of a length (**Chwang et al., 1983**). σ_0 ranges from 0 to infinity. When $\sigma_0 = 0$, the upper damping plate is totally impermeable. Conversely, the upper damper vanishes as the σ_0 tends to infinity. The porous boundary condition based on Darcy's law specifies that the normal fluid velocity passing through a thin porous plate is linearly proportional to the pressure difference between the two sides of the plate consistent with the linear assumption (**Taylor et al., 1956; Chwang et al., 1983**).

In addition to the boundary conditions in different regions, matching conditions are required for the continuity of fluid solutions in adjacent regions (Region I and Region III, Region II and Region III) as follows:

$$\phi_1 = \phi_3 \qquad \text{for} \quad 0 \geq z \geq -b_2, \quad r = a_2 \tag{2.6-a}$$

$$\frac{\partial \phi_1}{\partial r} = \frac{\partial \phi_3}{\partial r} \qquad \text{for} \quad 0 \geq z \geq -b_2, \quad r = a_2 \tag{2.6-b}$$

$$\phi_2 = \phi_3 \qquad \text{for} \quad -b_2 \geq z \geq -h, \quad r = a_2 \tag{2.6-c}$$

$$\frac{\partial \phi_2}{\partial r} = \frac{\partial \phi_3}{\partial r} \qquad \text{for} \quad -b_2 \geq z \geq -h, \quad r = a_2 \tag{2.6-d}$$

The above matching conditions ensure the continuity of velocity (Eq. 2.6-b & Eq. 2.6-d) and continuity of pressure (Eq. 2.6-a & Eq. 2.6-c) across the boundary $r = a_2$ (**Ning et al., 2017; Sarkar et al., 2020; Wang et al., 2021**).

2.2 Analytical solutions in sub-regions

By applying the Helmhotz equation, variables of velocity potential could be separated in each region (**Linton et al., 2001**), and analytical solutions for the wave diffraction problem are derived. The velocity potential ϕ_3 for Region III can be written by using the eigen-function expansions like followings:

$$\begin{aligned}\phi_3(r,\theta,z) &= \phi_i + \phi_d \\ &= -\frac{igA}{\omega}\sum_{m=0}^{\infty}\varepsilon_m \cos(m\theta)\left[i^m J_m(k_0 r) Z_0(k_0 z)\right. \\ &+ \left.\sum_{j=0}^{\infty} A_{mj}\, Z_j(k_j z) U_m(k_j r)\right]\end{aligned} \tag{2.7}$$

with

$$\varepsilon_m = \begin{cases} 1; & m = 0, \\ 2; & m \geq 1, \end{cases} \tag{2.8}$$

where A_{mj} are the unknown coefficients, J_m represents the first kind of Bessel function of order m and A is the amplitude of the incident wave. In outer region, the velocity potential of the fluid consists of the incident waves and the diffraction waves. The velocity potential of the incident wave is written as the first term of Eq. 2.7 (**MacCamy and Fuchs 1954**). Here, wavenumber k_0 and k_j (j=1, 2, 3 …) are derived by using the following dispersion relations (**Linton et al., 2001; Chamberlain and Porter 1999**):

$$\omega^2 = \begin{cases} gk_j tanhk_j h; & j = 0, \\ -gk_j tank_j h; & j \geq 1, \end{cases} \tag{2.9}$$

The radial eigen-functions $U_m(k_j r)$ in Region III are given as follows:

$$U_m(k_j r) = \begin{cases} \dfrac{H_m(k_j r)}{H_m(k_j a_2)}; & j = 0, \\ \dfrac{K_m(k_j r)}{K_m(k_j a_2)}; & j \geq 1, \end{cases} \tag{2.10}$$

where $H_m(k_j r)$ represents the Hankel function of first kind of order m and $K_m(k_j r)$ is the second kind of modified Bessel function of order m. The vertical eigen-function $Z_j(k_j z)$ in Region III are defined as:

$$Z_j(k_j z) = \begin{cases} \dfrac{\cosh[k_j(z+h)]}{\cosh(k_j h)}; & j = 0, \\ \dfrac{\cos[k_j(z+h)]}{\cos(k_j h)}; & j \geq 1, \end{cases} \tag{2.11}$$

The velocity potential ϕ_2 in the bottom region (Region II) can be derived by satisfying the sea-bed and body boundary conditions (Eq. 2.4):

$$\phi_2(r,\theta,z) = -\frac{igA}{\omega} \sum_{m=0}^{\infty} \varepsilon_m \cos(m\theta) \sum_{j=0}^{\infty} \varepsilon_m C_{mj}\, Y_j(\gamma_j z) V_m(\gamma_j r) \tag{2.12}$$

where C_{mj} are the unknown coefficients. The radial eigen-functions $V_m(\gamma_j r)$ in Region II are derived with the consideration of boundedness condition,

namely

$$V_m(\gamma_j r) = \begin{cases} \left(\frac{r}{a_2}\right)^j; & j = 0, \\ \frac{I_m(\gamma_j r)}{I_m(\gamma_j a_2)}; & j \geq 1, \end{cases} \tag{2.12}$$

where $I_m(\gamma_j r)$ denotes the Bessel function of first kind of order m. In this case, Eigenvalues γ_j can be computed from:

$$\gamma_j = \frac{j\pi}{h - b_2} \tag{2.13}$$

The vertical eigen-function $Y_j(\gamma_j z)$ in Region II are given as follows:

$$Y_j(\gamma_j z) = \begin{cases} 1; & j = 0, \\ \cos[\gamma_j(z + h)]; & j \geq 1, \end{cases} \tag{2.14}$$

The scattered velocity potential in Region I, which satisfies the linear free surface boundary condition, impermeable and permeable body boundary conditions, has the form:

$$\phi_1(r, \theta, z) = -\frac{igA}{\omega} \sum_{m=0}^{\infty} \varepsilon_m \cos(m\theta) \sum_{j=0}^{\infty} B_{mj} f(\kappa_j z) W_m(\kappa_j r) \tag{2.15}$$

where B_{mj} are the unknown coefficients. The radial eigen-function $W_m(\kappa_j r)$ is derived by satisfying the horizontal body boundary condition on the sidewall

of the truncated cylinder, namely

$$W_m(\kappa_j r) = \frac{H'_m(\kappa_j a_1)J_m(\kappa_j r) - J'_m(\kappa_j a_1)H_m(\kappa_j r)}{H'_m(\kappa_j a_1)J_m(\kappa_j a_2) - J'_m(\kappa_j a_1)H_m(\kappa_j a_2)} \tag{2.16}$$

where $J_m(\kappa_j r)$ and $H_m(\kappa_j r)$ denotes the Bessel function of first kind of order m. J'_m and H'_m denote the first derivative of the first kind of Bessel function and Hankel function of order m, respectively.

By satisfying the appropriate boundary conditions as well as the continuity of the normal velocity through the porous damping plate in Region I, the vertical eigen-function $f(\kappa_j z)$ could be derived as:

$$f(\kappa_j z) = \begin{cases} \sinh[\kappa_j(b_2 - b_1)]\,[\kappa_j \cosh(\kappa_j z) + \nu \sinh(\kappa_j z)]; 0 \geq z \geq -b_1, \\ \mathrm{X}(\kappa_0 b_1)\cosh[\kappa_j(z + b_2)]; b_1 \geq z \geq -b_2, \end{cases} \tag{2.17}$$

where $\mathrm{X}(\kappa_0 z)$ is defined as: $\mathrm{X}(\kappa_j z) = \nu \cosh(\kappa_j z) - \kappa_j \sinh(\kappa_j z)$. The eigenvalues κ_j are the roots of:

$$\kappa_j\, \mathrm{X}(\kappa_j b_1)\sinh[\kappa_j(b_2 - b_1)] = i\sigma_0 \mathrm{X}(\kappa_j b_2) \tag{2.18}$$

Such eigenvalues κ_j yield a special dispersion relation for the evanescent wave by satisfying the porous boundary condition in the vertical direction. Different from the conventional dispersion relation for the impermeable sea bed and horizontal damper, the roots of this transcendental equation (Eq. 2.18) are complex number instead of real or pure imaginary numbers. It is worth to

mention about two special cases before solving Eq. 2.18 to obtain the complex wave number.

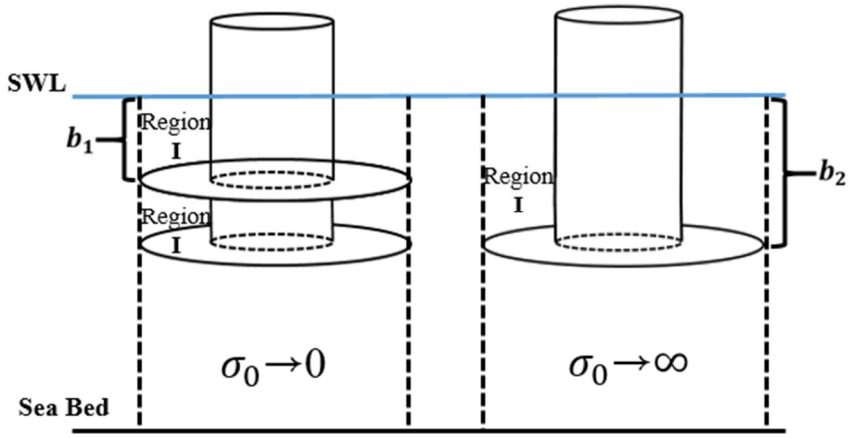

Figure 2.3 Schematic of dual damping plate w.r.t. different porous effect parameter

Firstly, when the porous effect parameter σ_0 vanishes, the upper damping plate is totally impermeable without any pores as illustrated in the left of Fig. 2.3. As a result, right hand side of Eq. 2.18 vanishes. Thus, the local fluid above the upper damper is under a shallow water effect of depth b_1, and the equation of dispersion relation will change into

$$\mathrm{X}(\kappa_j b_1) = \nu \cosh(\kappa_j b_1) - \kappa_j \sinh(\kappa_j b_1) = 0 \tag{2.19-a}$$

or

$$\sinh[\kappa_j(b_2 - b_1)] = 0 \tag{2.19-b}$$

In this case, the local fluid between two impermeable damping plate is identical to the fluid in Region II, and a set of eigenvalues could be obtained as $j\pi/(b_2 - b_1)$.

Secondly, when the porous effect parameter σ_0 tends to infinity, the upper damping plate is fully permeable, as illustrated in the right of Fig. 2.3, which means the upper damper vanishes. As a result, the conventional dispersion relation of shallow water of depth b_2 is suitable for the local fluid in Region I. The roots of eigenvalues κ_j could be found from:

$$\mathrm{X}(\kappa_j b_2) = \nu \cosh(\kappa_j b_2) - \kappa_j \sinh(\kappa_j b_2) = 0 \tag{2.20}$$

As the porous effect parameter σ_0 changes from 0 to infinity, the roots of eigenvalues κ_j begins from the roots of Eq. 2.19, which consist of one real wave number (Eq. 2.19-a) and a group of pure imaginary solutions (Eq. 2.19-b). As porosity increases, the roots of κ_j changes gradually toward to the roots of Eq. 2.20. Due to the behavior of eigenvalues mentioned above, iteration method is applied to compute the roots of κ_j.

Newton Raphson iteration method for complex roots (**Muheadden et al., 2010)** is chosen in the present work to solve the roots of eigenvalues κ_j with respect to various porous effect parameters σ_0. The Complex Newton Raphson iteration method is defined as below:

$$z_{k+1} = z_k - \frac{f(z_k)}{f'(z_k)} \tag{2.21-a}$$

$$(x+iy)_{k+1} = (x+iy)_k - \frac{f((x+iy)_k)}{f'((x+iy)_k)} \tag{2.21-b}$$

$$x_{k+1} + iy_{k+1} = \left[x_k - \frac{f(x_k)}{f'(x_{k+1})}\right] + i\left[y_k - \frac{f(y_k)}{f'(y_{k+1})}\right] \tag{2.21-c}$$

Before implementing iterations, it is necessary to find a group of appropriate initial guesses for each root of equation to avoid skipping solutions. Generally, the zero dissipation root (ZDR) is mostly used as an initial guess (**Liu et al., 1973; McIver et al., 1998; Mendez et al., 2004**), which assumes that the upper damping plate is totally impermeable (Eq. 2.19). After obtaining the first group of roots, the porous effect parameter σ_0 will be increased by a very small step and then the first group of roots will be used as a new set of initial guesses. By repeating this procedure and increasing the porous effect parameter σ_0 gradually to the target porosity, the final complex roots of eigenvalues κ_j could be computed. Fig. 2.4 shows a case of relation between initial guess and final solutions.

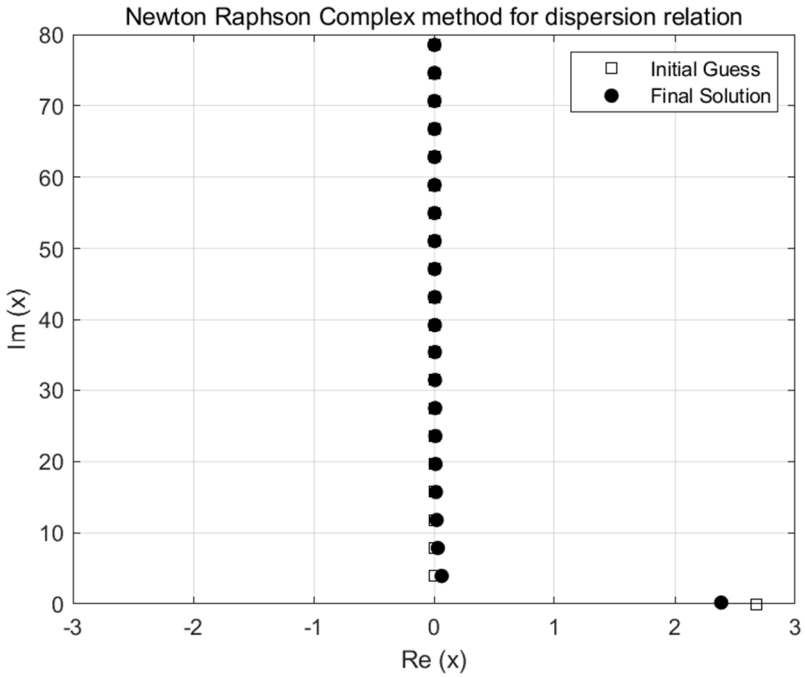

Figure 2.4 Behavior of roots for the porous damping pate dispersion relationship using Newton's method

2.3 Computation of unknown coefficients

The vertical eigen-functions in different sub-regions form orthogonal sets between their upper boundary and bottom boundary. Regarding to the vertical eigen-function in Region I, it leads to the following integrals:

$$\int_{-b_2}^{0} f(\kappa_p z) f(\kappa_q z) dz = 0 \quad (p \neq q) \tag{2.22}$$

By using the matching condition for pressure continuity given by Eq.2.6-a for the depth $0 \geq z \geq -b_2$, along with the orthogonal property of vertical eigen-function $f(\kappa_j z)$ in Region I, we could obtain:

$$\sum_{j=0}^{\infty} A_{mj} E_{j\alpha} - B_{mj} F_{\alpha} = -i^m J_m(k_0 a_2) E_{0j} \tag{2.23}$$

Using the matching conditions for pressure continuity given by Eq.2.6-c for the depth $-b_2 \geq z \geq -h$ and the orthogonal property of vertical eigen-function $Y_j(\gamma_j z)$ in Region II, we could get:

$$\sum_{j=0}^{\infty} A_{mj} G_{j\alpha} - C_{mj}(h-d) = -i^m J_m(k_0 a_2) G_{0j} \tag{2.24}$$

Regarding the velocity continuity, by using the matching conditions given by Eq.2.6-b,d for the depth $0 \geq z \geq -h$ and the orthogonal property of vertical eigen-functions $Z_j(k_j z)$ in Region III, we could get:

$$A_{mj}U'_m(k_j a_2)L_j - \sum_{j=0}^{\infty} B_{mj}W'_m(\kappa_j a_2)E_{\alpha j}$$
$$-\sum_{j=0}^{\infty} C_{mj}\varepsilon_m V'_m(\gamma_j a_2)G_{\alpha j} = -\delta_{j0} i^m k_0 J'_m(k_0 a_2)L_j \tag{2.25}$$

where δ is the Dirac delta function, which is defined as below:

$$\delta_{\mathrm{pq}} = \begin{cases} 1; & p = q, \\ 0; & p \neq q, \end{cases} \tag{2.26}$$

$E_{\alpha j}$, F_α, $G_{\alpha j}$ and L_j represent the integrals of vertical eigen-function of variable, which are defined as:

$$E_{j\alpha} = \int_{-b_2}^{0} Z_j(k_j z) f(\kappa_\alpha z)\, dz \tag{2.27-a}$$

$$F_\alpha = \int_{-b_2}^{0} f(\kappa_\alpha z) f(\kappa_\alpha z)\, dz \tag{2.27-b}$$

$$G_{j\alpha} = \int_{-b_2}^{0} Z_j(k_j z) Y_\alpha(\gamma_\alpha z)\, dz \tag{2.27-c}$$

$$L_j = \int_{-h}^{0} Z_j(k_j z) Z_j(k_j z)\, dz \tag{2.27-d}$$

To obtain wave run-up and wave loads acting on the truncated cylinder, it is necessary to truncated the infinite series (Eq.2.23-25) to finite terms. Then, three sets of algebraic equations could be solved by using the standard matrix techniques and thereby the complex coefficients A_{mj}, B_{mj} and C_{mj} could be

obtained. Finally, the velocity potentials of fluid in different regions could be uniquely determined.

2.4 Computations of wave run-up and hydrodynamic forces

Once the formulation of velocity potentials in each region are obtained, wave run-up around the truncated cylinder could be calculated by using the velocity potentials. The relationship between velocity potential and wave elevation is given as:

$$\eta = -\frac{1}{g}\frac{\partial \Phi(r,\theta,z,t)}{\partial t} \tag{2.28}$$

where $\Phi(r,\theta,z,t) = Re\left[\phi(r,\theta,z)e^{-i\omega t}\right]$. The surge and heave wave exciting forces acting on the truncated cylinder could be calculated by integrating the hydrodynamic pressure on the wetted body surface according to Eq. 2.29. Note that since the thickness of dual damping plate is assumed as zero, there is no hydrodynamic load in the x direction (surge force) acting on the damping plates.

$$F_1 = \iint_{S_{a_1}} pn_x ds = i\omega\rho \int_{-b_2}^{0}\int_{0}^{2\pi} \phi_1 cos\theta dz d\theta \tag{2.29}$$

Regarding to the heave wave exciting force, the total loads could be separated into two components: F_{31} and F_{32}, which represent the vertical forces acting on surface of upper porous damping plate $(z = -b_1, a_1 < r < a_2)$ and surface of lower impermeable damping plate $(z = -b_2, 0 < r < a_2)$, respectively. The expressions are given by:

$$F_{3=}F_{31} + F_{32} \tag{2. 30-a}$$

$$F_{31} = \iint_{S_{b_1}} pn_z ds$$

$$= -i\omega\rho \int_{a_1}^{a_2} \int_0^{2\pi} (\phi_1(r, -b_1^+, \theta) - \phi_1(r, -b_1^-, \theta)) r dr d\theta \tag{2. 30-b}$$

$$F_{32} = \iint_{S_{b_2}} pn_z ds \tag{2. 30-c}$$

$$= -i\omega\rho[\int_{a_1}^{a_2} \int_0^{2\pi} \phi_1(r, -b_2, \theta) r dr d\theta$$

$$- \int_0^{a_2} \int_0^{2\pi} \phi_2(r, -b_2, \theta) r dr d\theta$$

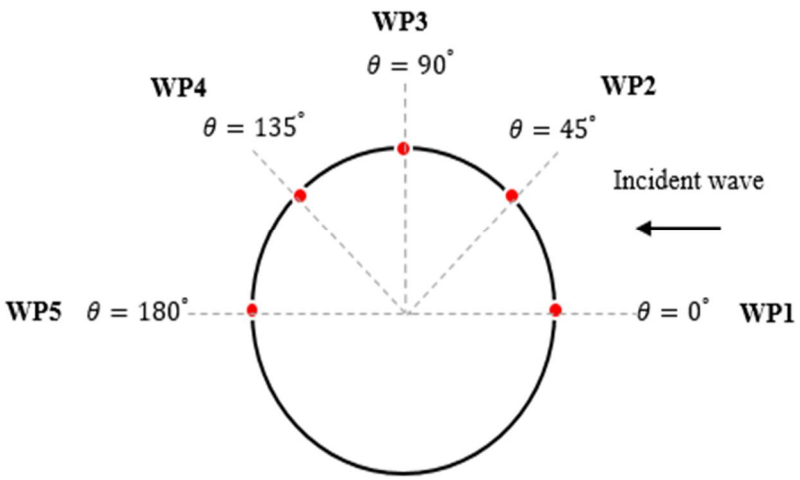

Figure 2.5 Position of wave probes on the truncated cylinder

To check the convergence of present MEEM solution, the normalized wave run-up around the truncated cylinder with dual thin damping plate are examined

with respect to different truncated numbers *N*. As illustrated in Fig.2.5, five wave probes are attached on the surface of the truncated cylinder at the calm water level. The wave probes are installed at 0° , 45° , 90° , 135° and 180° with respect to the direction of incident wave. The behavior of convergence for the truncated cylinder with different dual damping plate are given in Table 2.2, where the $b_0 = 10$. Here, $b_0 = 2\pi\sigma_0/k_0$ indicates the dimensionless porous effect parameter of the upper damping plate. This table shows that the convergence of the calculation results is very rapid. The truncated number of *N*=20 can yield three decimals accuracy with the consideration of porous structure. As a results, *N*=20 will be used throughout the present numerical study.

Table 2.2 Convergence study of normalized wave run-up η/A around the truncated cylinder with dual dampers for ka=0.2

Truncated number *N*	Dimensionless wave run-up				
	$\frac{b_1}{b_2} = 0.7, \frac{b_2}{h} = 0.1, \frac{a_1}{a_2} = 0.5, \frac{a_1}{h} = 0.03, b_0 = 10$				
	WP1	WP2	WP3	WP4	WP5
0	1.05885	1.01668	0.96812	1.00172	1.03849
1	1.03973	1.01499	0.98503	0.99955	1.01893
5	1.04768	1.02090	0.98676	0.99987	1.01916
10	1.04506	1.01805	0.98358	0.99679	1.01625
15	1.04077	1.01423	0.98064	0.99427	1.01375
16	1.04004	1.01357	0.98009	0.99374	1.01320
17	1.03940	1.01297	0.97953	0.99314	1.01257
18	1.03889	1.01247	0.97901	0.99254	1.01192

19	1.03858	1.01214	0.97861	0.99217	1.01136
20	1.03849	1.01201	0.97837	0.99203	1.01132

3. Validation of Numerical Method

To validate the present MEEM solutions, a comparison of wave run-up and hydrodynamic loads acting on the structures with other computational results for other porous structures was conducted. Furthermore, the wave elevations around the truncated cylinder with various types of damping plates were compared with boundary element method (BEM) solutions. This validation work is divided into two sections: a truncated cylinder with an impermeable damping plate and a truncated cylinder with a porous damping plate.

3.1 Case I: Truncated cylinder with impermeable damping plate

Regarding the wave run-up around the truncated cylinder with an impermeable damping plate, the present MEEM solutions are compared to BEM solutions by using WADAM program. WADAM is a comprehensive hydrodynamic analysis program designed to calculate wave-structure interaction for both fixed and floating structures of arbitrary shape.

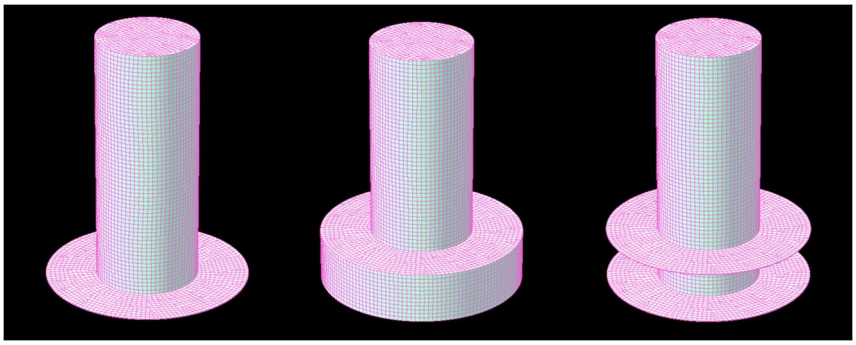

Figure 3.1 Panel model of truncated cylinder with three types of damping plate

The target impermeable panel models used for validation, as shown in Fig.3.1, are the truncated cylinder with a single thin damper, a single thick damper, and dual thin dampers. The dimensions of truncated cylinders and damping plates are given in Table 2.1. In the present MEEM method, the thickness of thin damper is assumed to be zero, while the thickness of thin damper in WADAM is set as 0.1m.

Fig 3.2 shows a comparison of wave run-up around the truncated cylinder with single thin damping plate between present MEEM solution and BEM solutions. The wave elevations are non-dimensionalized by the amplitude of the incident wave A. The x axis indicates the scattering parameter ka, where k and a represent the incident wave number and the radius of the truncated cylinder, respectively. It can be seen that there is a good agreement between the MEEM and BEM solutions. On the lee side of the truncated cylinder (WG1 & WG2), wave run-up increases as the scattering parameter increases until $ka = 0.9$. Conversely, on the weather side of the cylinder (WG4 & WG5), a weakly decreasing trend can be found as the scattering parameter increases.

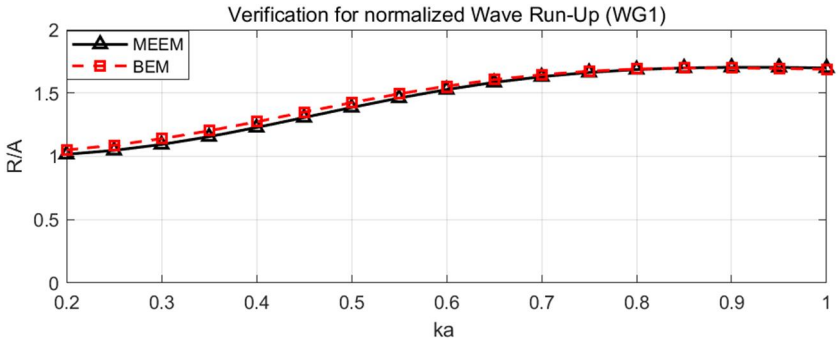
Verification for normalized Wave Run-Up (WG1)
MEEM
BEM
R/A
ka
0
0.5
1
1.5
2
0.2
0.3
0.4
0.5
0.6
0.7
0.8
0.9
1

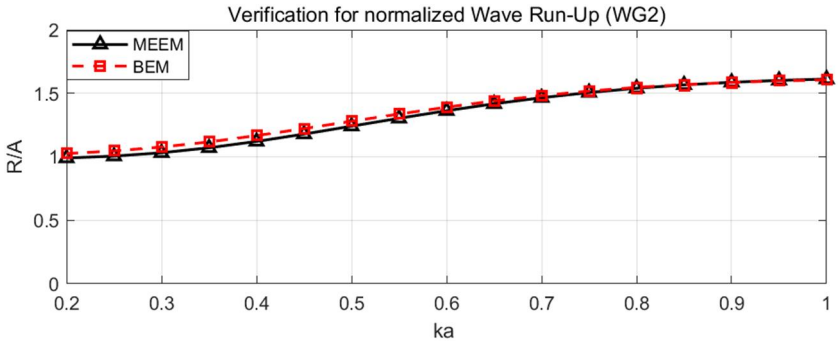
Verification for normalized Wave Run-Up (WG2)
MEEM
BEM
R/A
ka
0
0.5
1
1.5
2
0.2
0.3
0.4
0.5
0.6
0.7
0.8
0.9
1

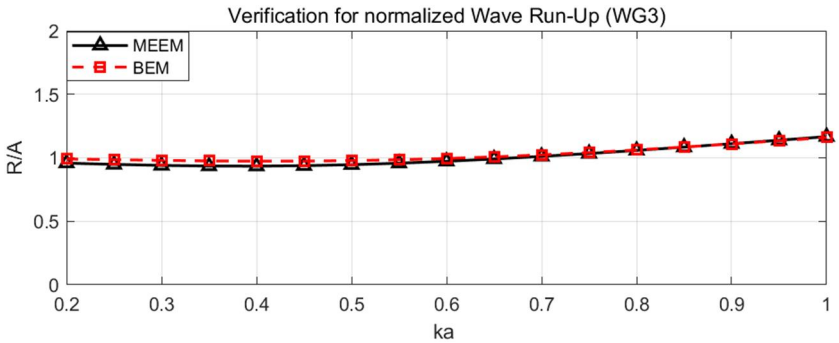
Verification for normalized Wave Run-Up (WG3)
MEEM
BEM
R/A
ka
0
0.5
1
1.5
2
0.2
0.3
0.4
0.5
0.6
0.7
0.8
0.9
1

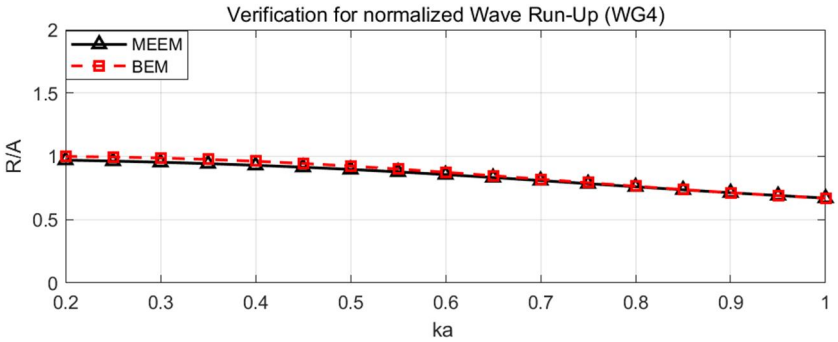

Figure 3.2 (Continued)

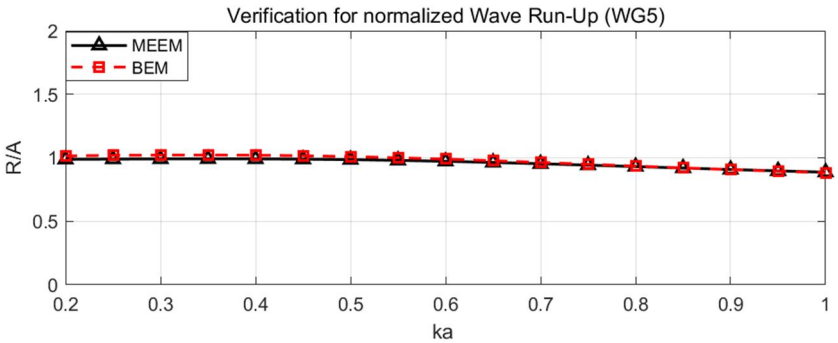

Figure 3.2 Comparison of wave run-up around truncated cylinder with single thin damper between present MEEM & BEM solution

Fig.3.3 and Fig.3.4 demonstrate the comparison of wave run-up around a truncated cylinder with dual thin dampers and a single thick damper, as computed by MEEM and BEM solutions, respectively. Present MEEM solutions agree well with the BEM solutions. Regarding the model used for validation, the separating distance of dual dampers and the thickness of thick damper are relatively small compared to the draft of the whole cylinder. Thus, the increments of wave run-up are not significant compared to the wave elevations around the cylinder with a single thin damper,

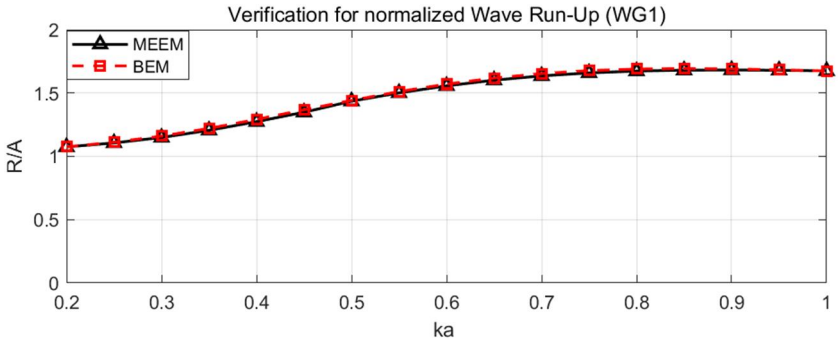
Verification for normalized Wave Run-Up (WG1)
MEEM
BEM
R/A
ka
0
0.5
1
1.5
2
0.2
0.3
0.4
0.5
0.6
0.7
0.8
0.9
1

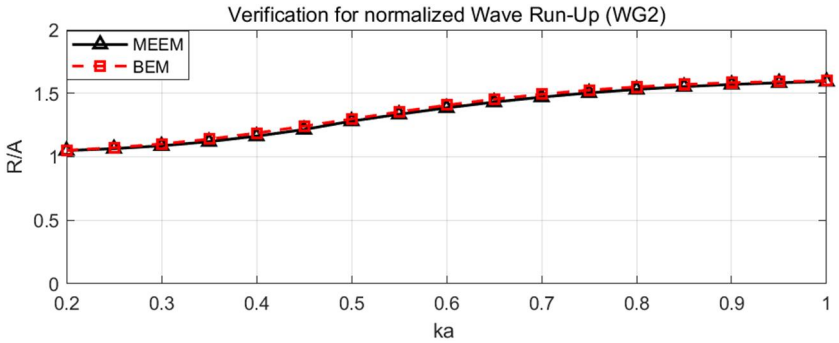
Verification for normalized Wave Run-Up (WG2)
MEEM
BEM
R/A
ka
0
0.5
1
1.5
2
0.2
0.3
0.4
0.5
0.6
0.7
0.8
0.9
1

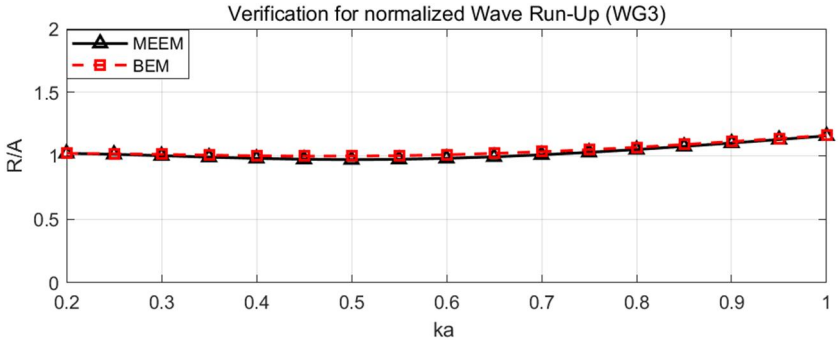
Verification for normalized Wave Run-Up (WG3)
MEEM
BEM
R/A
ka
0
0.5
1
1.5
2
0.2
0.3
0.4
0.5
0.6
0.7
0.8
0.9
1

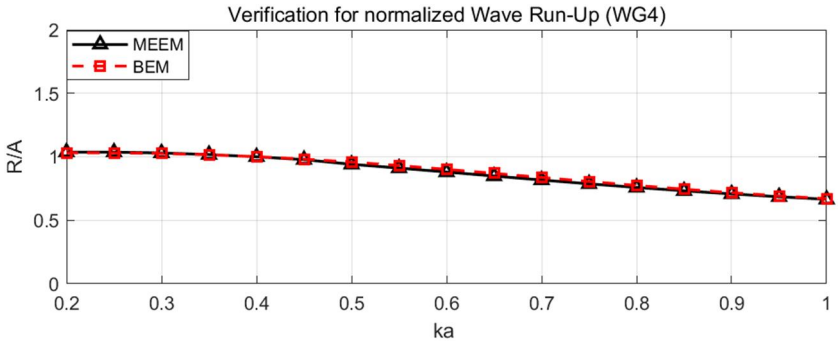
Verification for normalized Wave Run-Up (WG4)
MEEM
BEM
R/A
ka
0
0.5
1
1.5
2
0.2
0.3
0.4
0.5
0.6
0.7
0.8
0.9
1

Figure 3.3 (Continued)

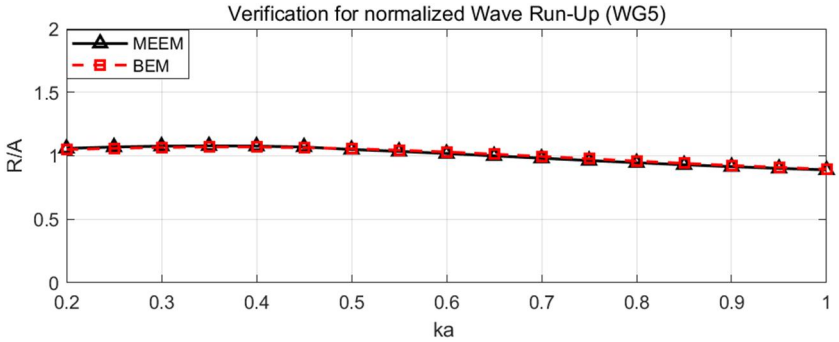

Figure 3.3 Comparison of wave run-up around truncated cylinder with dual thin dampers between present MEEM & BEM solution

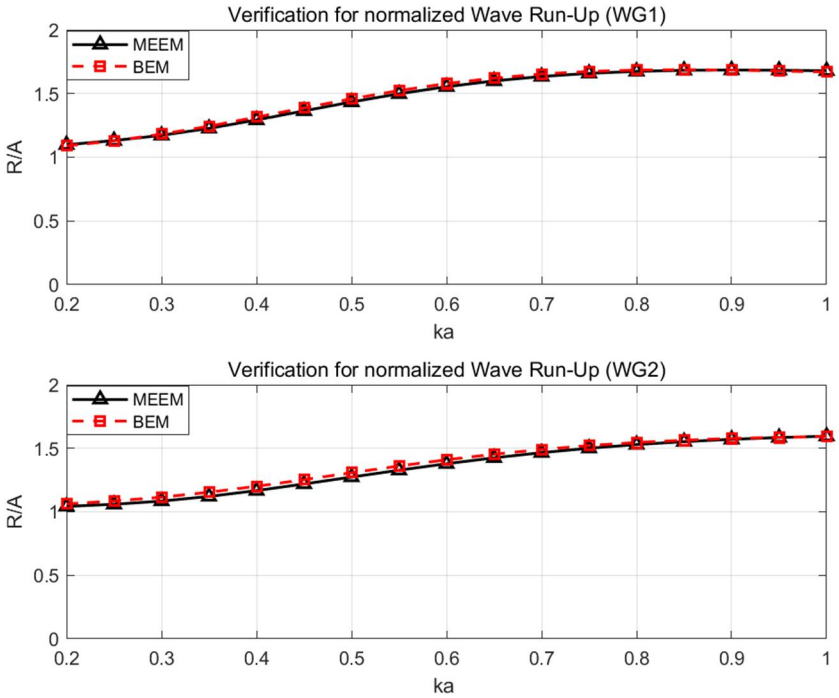

Figure 3.4(Continued)

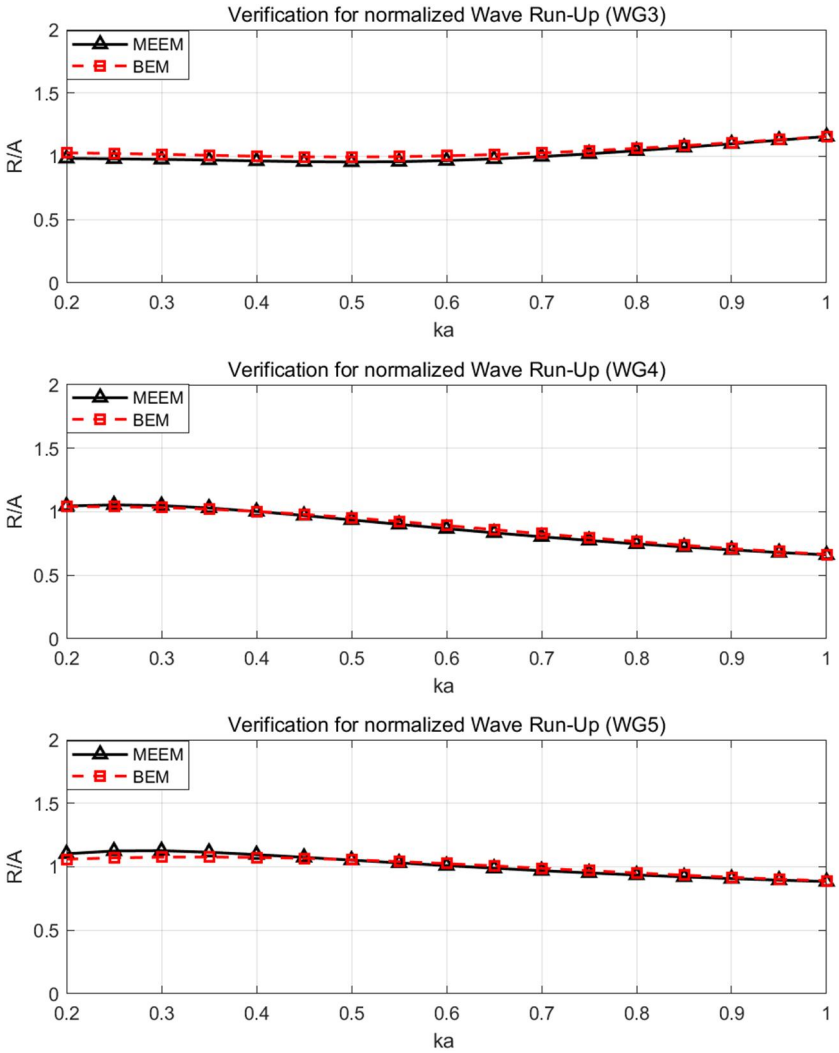

Figure 3.4 Comparison of wave run-up around truncated cylinder with single thick damper between present MEEM & BEM solution

3.2 Case II: Permeable structure

In this section, the present MEEM solutions for wave run-up and hydrodynamic loads acting on simple structures are compared with other computational results. As shown in Fig.3.5, three simple porous structures are used for validation in this work: a single horizontal porous membrane (Fig.3.5-a) (**Chwang et al., 1994, Cho et al., 2000**), a porous truncated cylinder with an inner porous plate (Fig.3.5-b) (**Bao et al., 2009**) and a porous truncated cylinder (Fig.3.5-c) (**Zhao et al., 2011**), respectively.

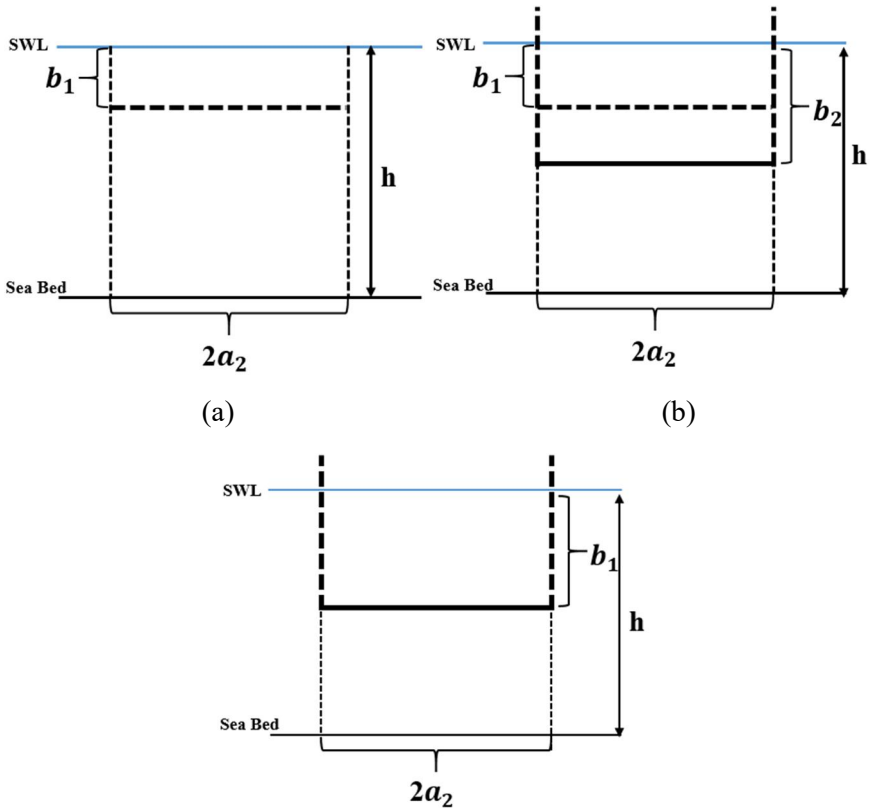

Figure 3.5 Schematic figure for three simple porous structures: (a) single horizontal porous membrane; (b) porous truncated cylinder with inner porous plate; (c) porous truncated cylinder

As previously noted, it is essential to select an appropriate truncated number in order to ensure the convergence of the analytical solution. For the structure with horizontal porous wall, the accurate computation of the complex wave number is necessary to ensure the accuracy of the analytical solutions. Different from the structure with vertical porous wall, horizontal porous wall can significantly influence the complex wave number. The real part of the complex wave number corresponds to the wave dispersion, while the imaginary part is related to dissipation (**Cho et al., 2000**). Consequently, prior to examining wave run-up around the simple porous structure, it is imperative to first identify the complex wave number.

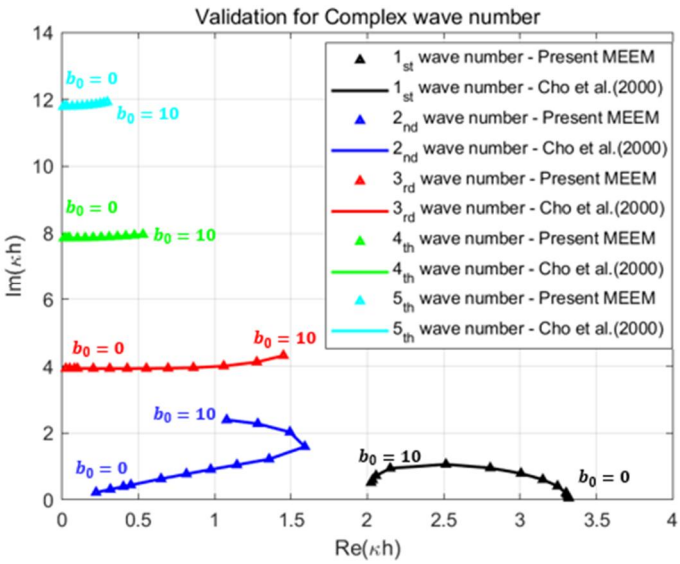

Figure 3.6 (Continued)

(a)

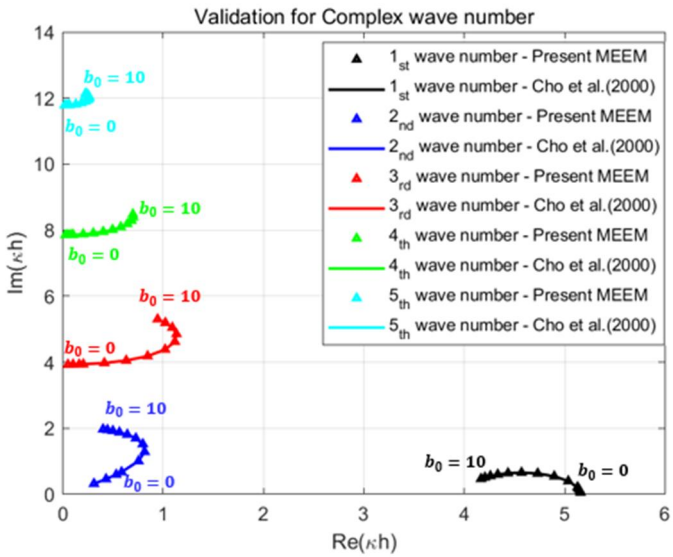

(b)

Figure 3.6 Validation for the complex wave numbers for first five modes: (a) $k_0h = 2.0$; (b) $k_0h = 4.0$ (k_0: wave number)

To validate the present solution for the complex wave number, the comparisons of the first five modes between the present solution and another 2-D analytical solution by **Cho et al. (2000)** are shown in Fig.3.6. Here, the target model is a horizontal porous membrane (Fig.3.5-a) with the geometric parameters $b_1/h = 0.2, a_2/h = 0.5, t/\rho g h^2 = 0.1$, where t is the wave period. Favorable agreement between present results and solutions of **Cho et al. (2000)** is obtained. Interestingly, for $k_0h = 4.0$, the real parts of the complex wave number in the higher-mode (3rd, 4th & 5th) initially increase as the normalized porous effect parameter b_0 increases, and then decreases as b_0 exceeds a

certain threshold. Therefore, an equivalent higher-mode complex wave number (real part) could be obtained with a different porosity. This phenomenon has also been mentioned by **Craik et al. (1985)** and **Dalrymple et al. (1991).** Moreover, for higher modes, the imaginary part of the complex wave number increases, which leads to more rapid dissipation. As the porous effect parameter tends to zero, the real part of the complex wave number vanishes and the evanescent waves stop propagating, forming standing waves.

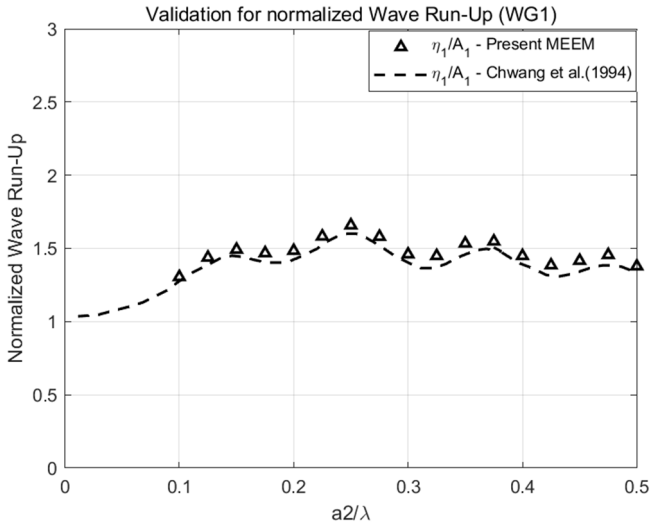

(a)

Figure 3.7 (Continued)

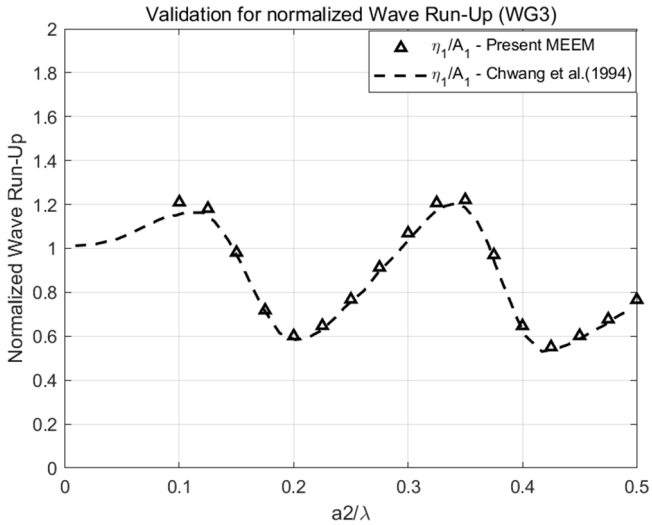

(b)

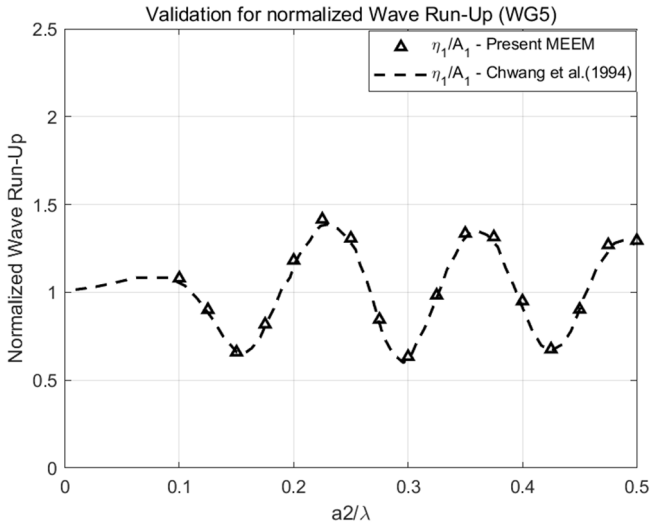

(c)

Figure 3.7 Validation for the wave elevation around a porous horizontal membrane: (a) Wave Probe 1 (0°); (b) Wave Probe 3 (90°); (c) Wave Probe 5 (180°)

Fig.3.7. illustrates the comparison between wave run-up computed by the

present MEEM solution and another analytical solution given by **Chwang et al. (1994).** Here, the target model is a horizontal porous disk (Fig.3.5-a), which is similar to the model proposed by **Cho et al. (2000).** The following parameters $\frac{b_1}{h} = 0.2, \frac{h}{\lambda} = 0.25, b_0 = 1.0$ have been set, where λ represents the wavelength. The present solutions show favorable agreement with **Chwang et al. (1994)**'s work. When the wavelength is quite long, the wave elevations around the porous disk are hardly disturbed by the existence of structure. Furthermore, when the porous effect parameter b_0 is very small, there is a wave focusing phenomenon. As the wavelength becomes longer, there exists a value of $\frac{a_2}{\lambda}$ at which wave focusing process is most significant, which was also mentioned by **Yu et al. (1993)**.

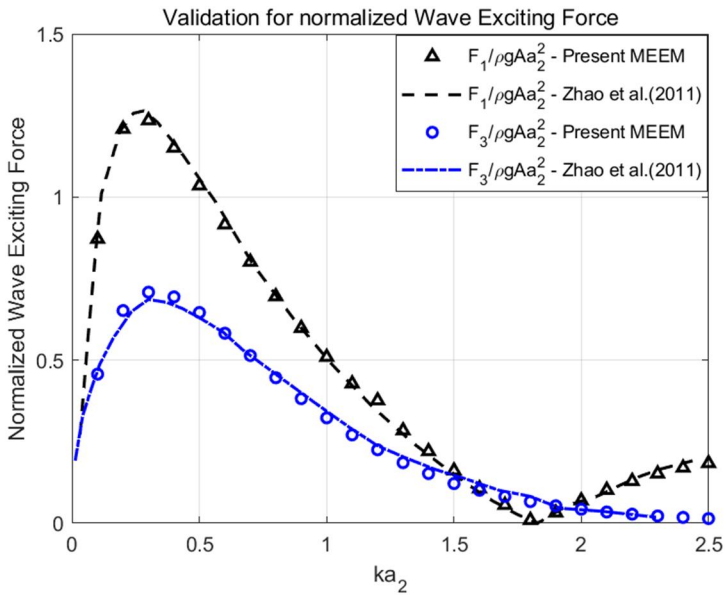

(a)

Figure 3.8 (Continued)

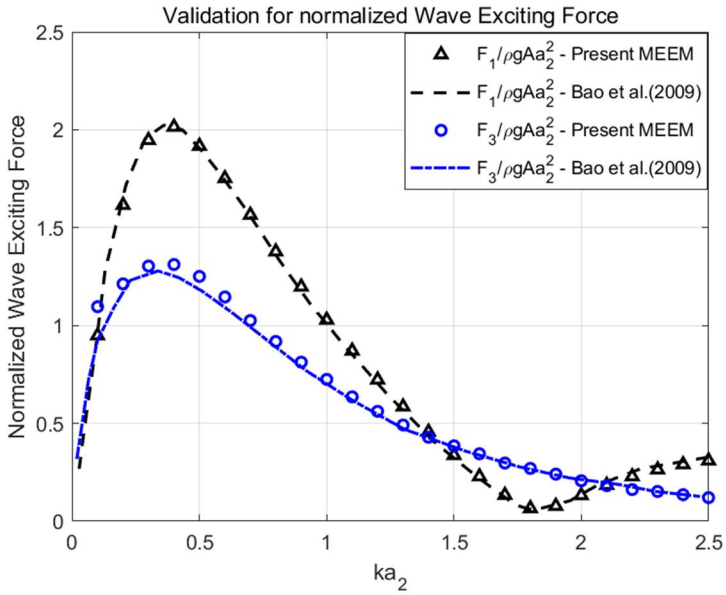

(b)

Figure 3.8 Validation for the surge and heave wave exciting force acting on porous structure: (a) porous truncated cylinder; (b) porous truncated cylinder with inner porous plate

Fig.3.8 shows the comparison between the hydrodynamic loads calculated by the present MEEM solutions and analytical solutions by **Bao et al. (2009) and Zhao et al. (2011).** Two examples are taken, namely a porous truncated cylinder with an inner porous plate (Fig.3.5-b) and a porous truncated cylinder (Fig.3.5-c). The geometric parameters for the porous truncated cylinder with an inner porous plate are set as $b_0 = 9, a_2/h = 0.03, b_1/h = 0.015$ and $b_2/h = 0.06$. The dimensions for the porous truncated cylinder are $b_0 = 9, a_2/h = 0.03, b_1/h = 0.06$. It is evident that the agreement between present evaluations and the results of **Bao et al. (2009) and Zhao et al. (2011).** As the scattering parameter increases, both the heave and surge wave exciting force initially increase, while then decline as ka continues to increase. When ka reaches

around 1.8, the surge exciting force approaches zero due to the emergence of the sloshing phenomenon inside the porous cylinder (**Zhao et al., 2011**). Consequently, the present computation of wave diffraction from truncated cylinder structures can be considered reliable.

4. Results and Discussion

To investigate the effect of damping plates on wave run-up around a truncated cylinder, this study considered three geometric parameters: the separating distance of dual damping plate, the thickness of single damping plate and the porosity of the upper damping plate.

4.1 Effect of Separation Distance

In this section, the effect of the separating distance between dual damping plates on wave run-up and wave exciting force will be analyzed. Here, both the upper and lower damping plates are assumed to be impermeable. The remaining parameters are set to $a_1/a_2 = 0.5, a_2/h = 0.06, b_2/h = 0.1, b_0 = 0.001$. Fig 4.1 shows the variation of the dimensionless wave run-up around the truncated cylinder versus the scattering parameter (ka) under various separating distance (d/D) conditions. Here d represents the separating distance between dual damping plates and D is the draught of the truncated cylinder.

As shown in Fig 4.1, wave elevations on both the lee side and the weather sides of a truncated cylinder increase as the separating distance of dual damping plates increases. This is due to the fact that the vertical distance between the upper plate and the still water level diminishes with an increase of separation distance, which results in a shallow water effect in the flow above the upper damping plate. Consequently, the evanescent waves become significant and the local flow is strongly generated.

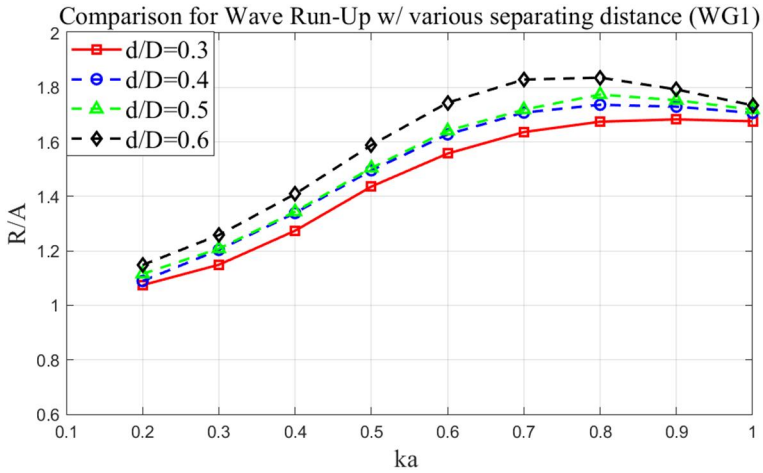
Comparison for Wave Run-Up w/ various separating distance (WG1)
d/D=0.3
d/D=0.4
d/D=0.5
d/D=0.6
R/A
ka

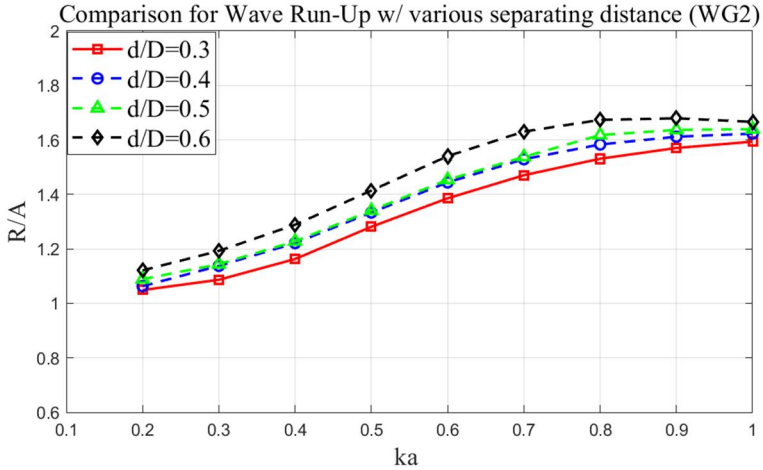
Comparison for Wave Run-Up w/ various separating distance (WG2)
d/D=0.3
d/D=0.4
d/D=0.5
d/D=0.6
R/A
ka

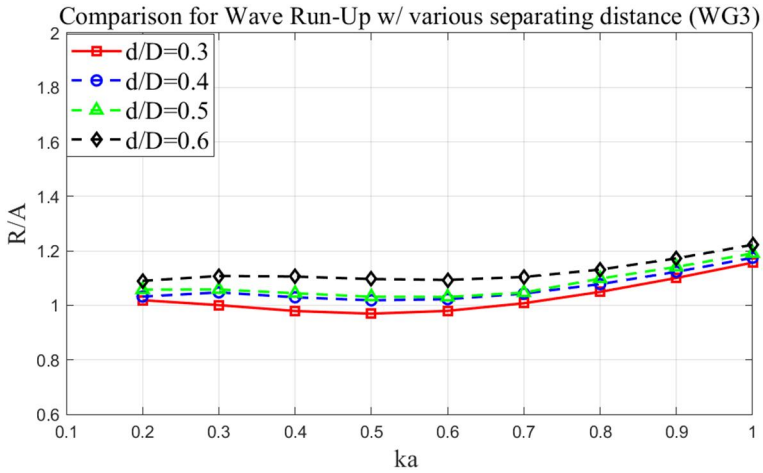
Comparison for Wave Run-Up w/ various separating distance (WG3)
d/D=0.3
d/D=0.4
d/D=0.5
d/D=0.6
R/A
ka

Figure 4.1 (Continued)

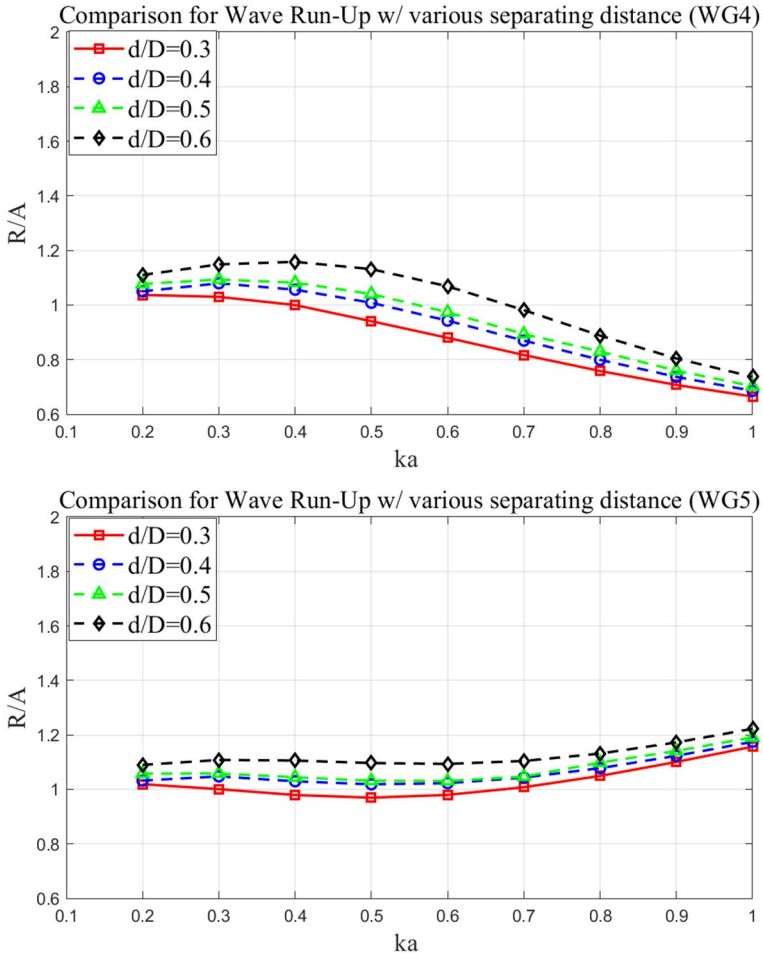

Figure 11 Comparison of wave run-up around the truncated cylinder with different separating distance d/D between dual dampers

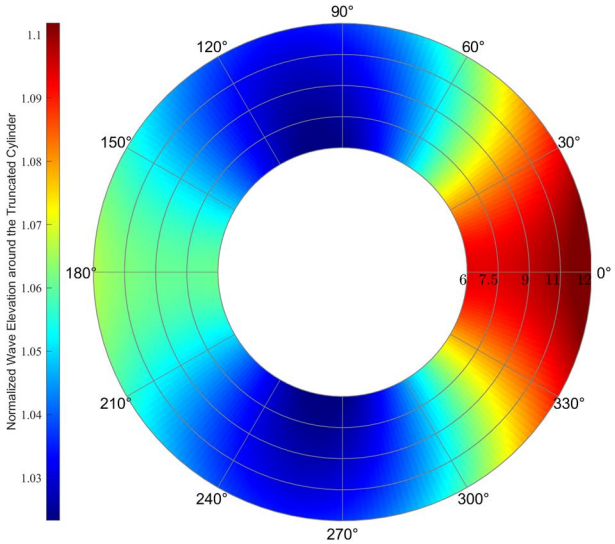

(a)

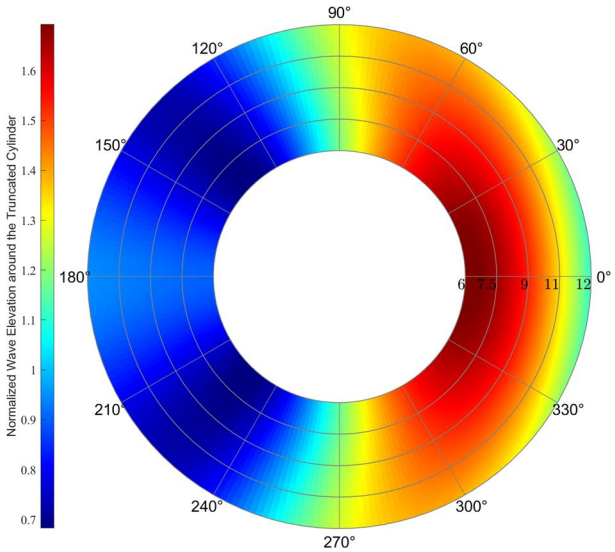

(b)

Figure 4.2 Distribution of wave amplitude around the truncated cylinder with impermeable dual damping plate ($d/D = 0.3$) with different scattering parameters: (a) ka=0.2; (b) ka=1

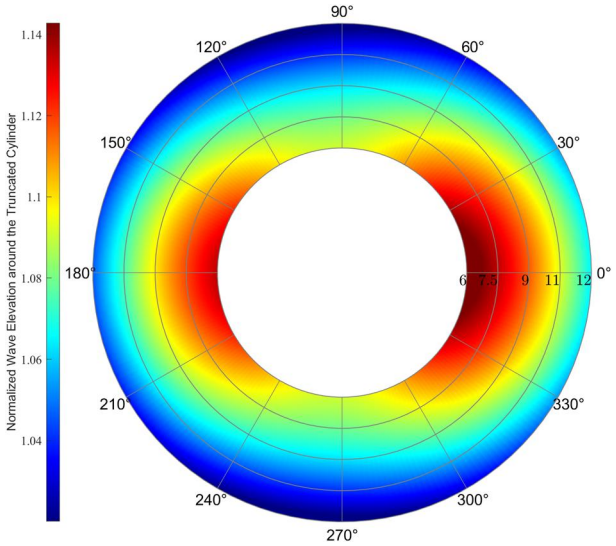

(a)

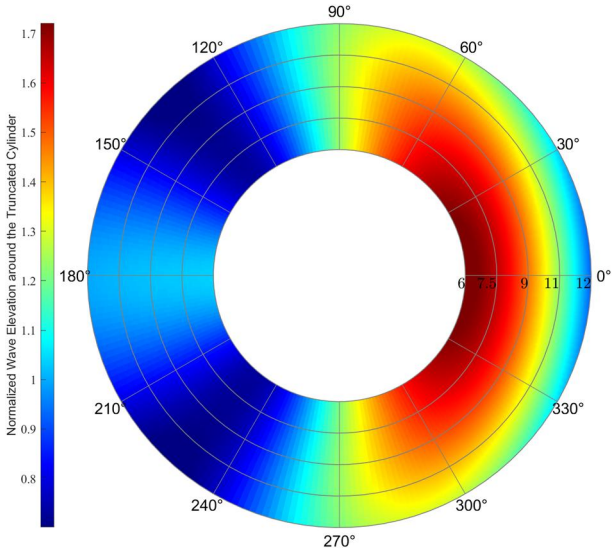

(b)

Figure 4.3 Distribution of wave amplitude around the truncated cylinder with impermeable dual damping plate ($d/D = 0.6$) with different scattering parameters: (a) ka=0.2; (b) ka=1

Fig 4.2 and Fig 4.3 demonstrate the distribution of wave amplitude around a truncated cylinder with the impermeable dual damping plate under different separating distance conditions. It is evident that when the wavelength of incident wave is short (ka=1), the wave elevations on the lee side are notably higher than those on the weather side of the truncated cylinder. Moreover, wave run-up of the cylinder gradually decreases from the front point (0°) to the back shoulder point (135°) of the cylinder. On the contrary, under the long wave conditions, the difference in water height between the lee side and weather side is not as large as the short wave cases. In addition, as the separating distance increases, wave run-up tends to be more symmetrically distributed on the lee side and weather side of the truncated cylinder. In summary, a larger separating distance between the impermeable dual damping plates can enhance wave run-up around the truncated cylinder.

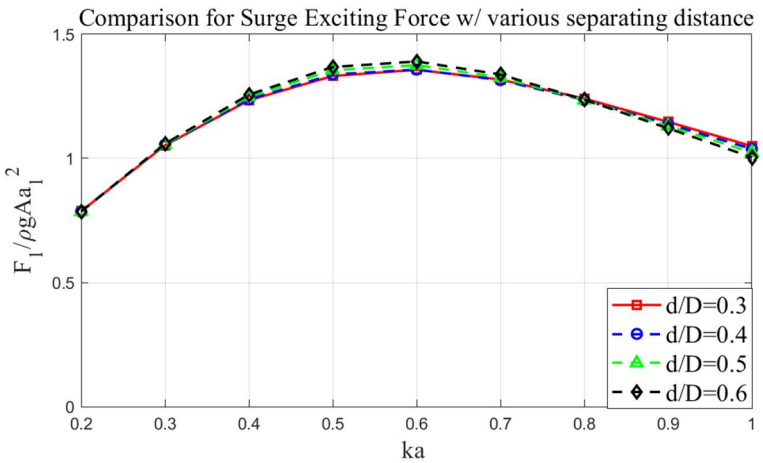

(a)

Figure 4.4 (Continued)

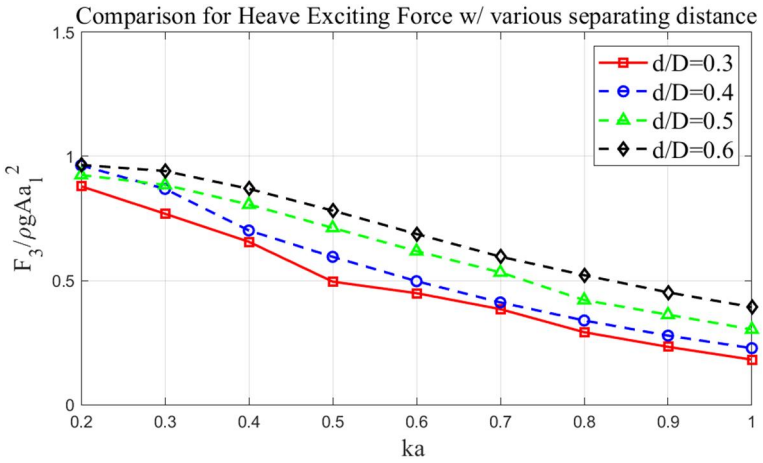

(b)

Figure 4.4 Comparison of wave exciting forces around the truncated cylinder with different separating distance d/D between dual dampers: (a) surge exciting force; (b) heave exciting force

The variation of surge and heave wave exciting forces acting on the truncated cylinder system versus the scattering parameter (ka) is illustrated in Fig.4.4 for various separating distances (d/D) between dual damping plates. As shown in Fig.4.4, the surge wave exciting force increases as the incident wave becomes shorter. When the scattering parameter is 0.6, the surge exciting force approaches maximum. Conversely, the heave wave exciting force continues to decrease as the scattering parameter increases. The surge wave exciting force is not significantly affected by the separating distances, whereas the heave wave exciting force reduces as the position of upper damping plate is lowered. This can also be attributed to the shallow water effect in the local fluid above and below the upper damping plate.

4.2 Effect of porosity

This section focuses on the influence of the porous effect parameter b_0 for the upper damping plate on wave run-up and wave exciting force. Again, the lower damping plate is assumed to be impermeable, with the remaining parameters $a_1/a_2 = 0.5, a_2/h = 0.06, b_2/h = 0.1$ also fixed. Fig 4.5 shows the variation of wave run-up around the truncated cylinder versus the scattering parameter ka when considering different porous effect parameter b_0 of the upper damping plate. Here the position of the upper porous damper is $b_1/h = 0.025$. The red solid line in the figures corresponds to the cases where upper damping plate is nearly impermeable. It is worth noting that, the normalized porous effect parameter of the upper damper is set to 0.001 instead of zero to avoid the singularity of the calculation.

As demonstrated in Fig 4.5, the porosity of the upper damping plate significantly affects the amplitude of wave elevations around the truncated cylinder. As the porosity parameter increases, the attenuating effects on wave run-up are strengthened, leading to a much lower wave run-up around the cylinder compared to the impermeable plate cases when the upper damping plate is highly porous. This porous effect is particularly evident under short wave condition. However, when the wavelength of the incident wave is very long, the wave elevations around the cylinder are not significantly affected by the porosity compared to the short waves. This is because when the wavelength of incident wave becomes very long (small *ka*), the characteristic length of the object is quite small compared to the incident wave, and thus the wave-body interaction becomes very weak.

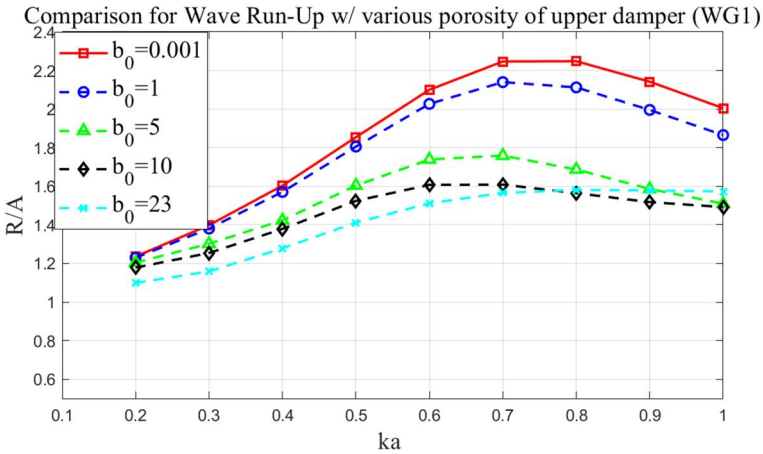
Comparison for Wave Run-Up w/ various porosity of upper damper (WG1)
b0=0.001
b0=1
b0=5
b0=10
b0=23
R/A
ka

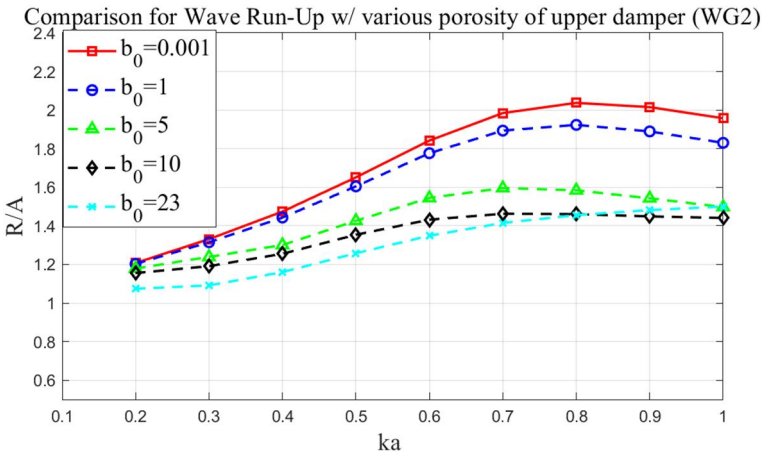
Comparison for Wave Run-Up w/ various porosity of upper damper (WG2)
b0=0.001
b0=1
b0=5
b0=10
b0=23
R/A
ka

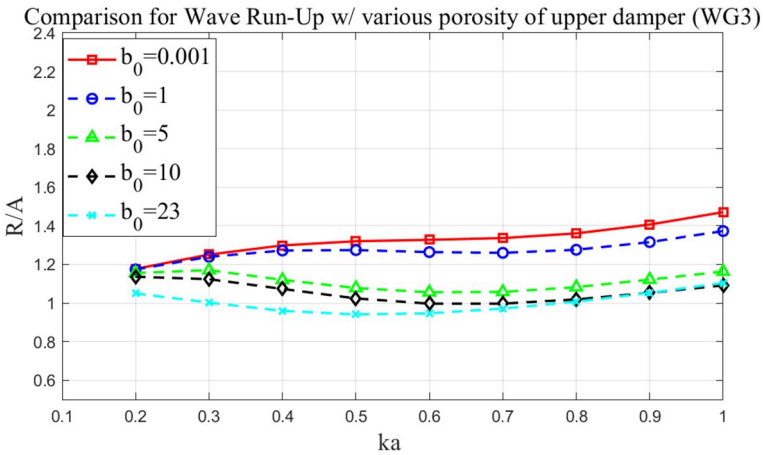
Comparison for Wave Run-Up w/ various porosity of upper damper (WG3)
b0=0.001
b0=1
b0=5
b0=10
b0=23
R/A
ka

Figure 4.5 (Continued)

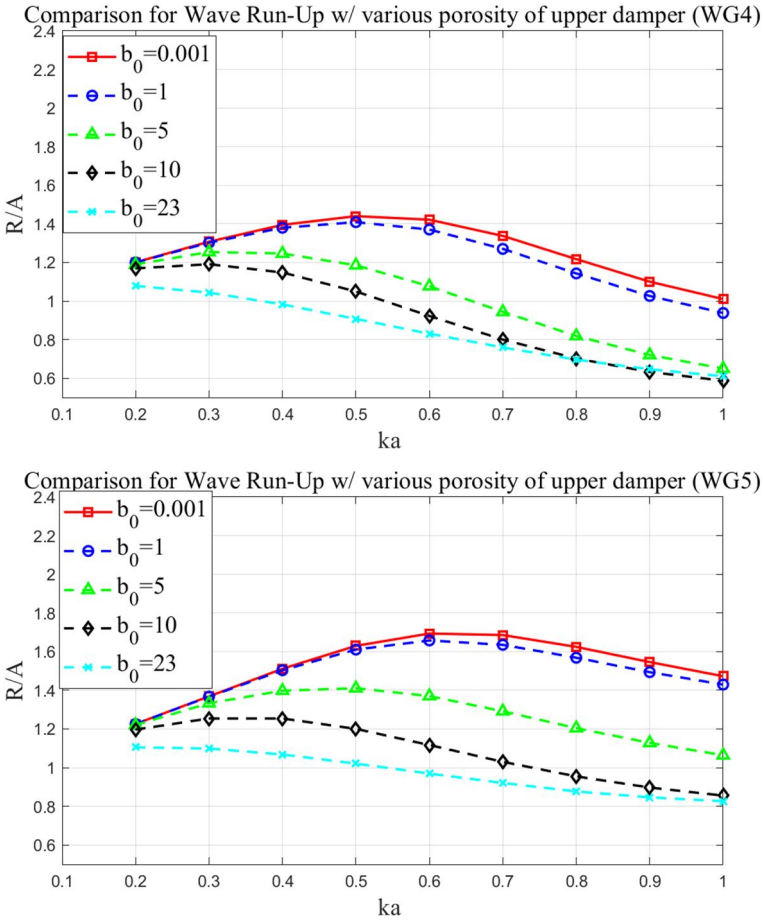

Figure 4.5 Comparison of wave run-up around the truncated cylinder with different b_0 for upper damper ($b_1/h = 0.025$)

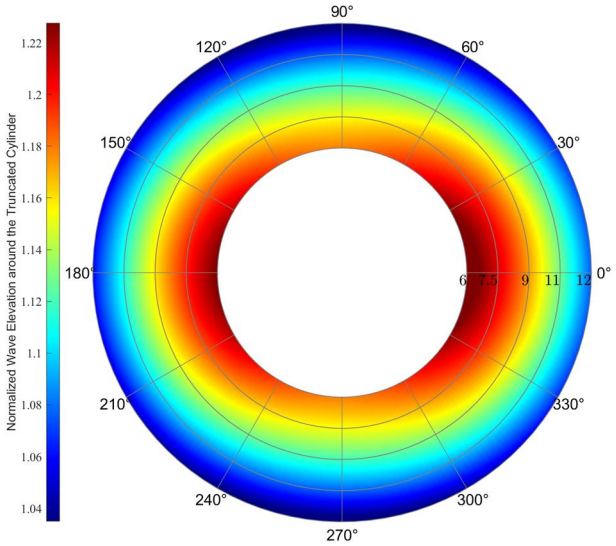

(a)

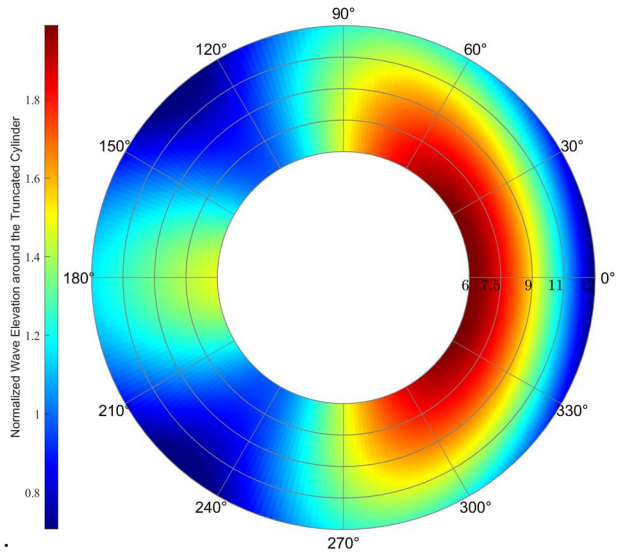

(b)

Figure 4.6 Distribution of wave amplitude around the truncated cylinder with porous dual damping plate ($b_0 = 0.001, b_1/h = 0.025$) with different scattering parameters: (a) ka=0.2; (b) ka=1

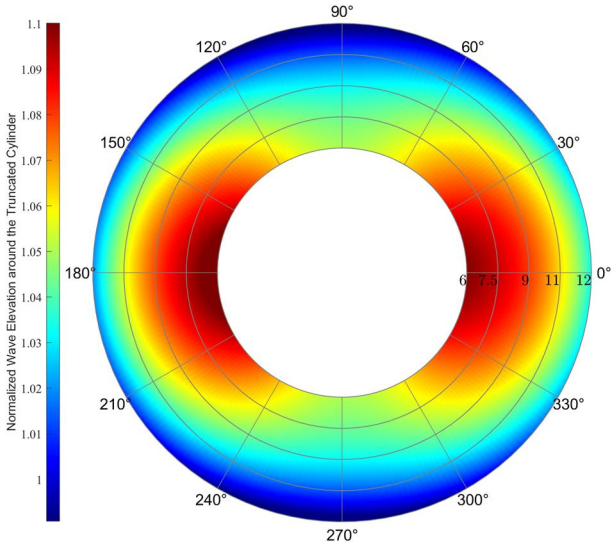

(a)

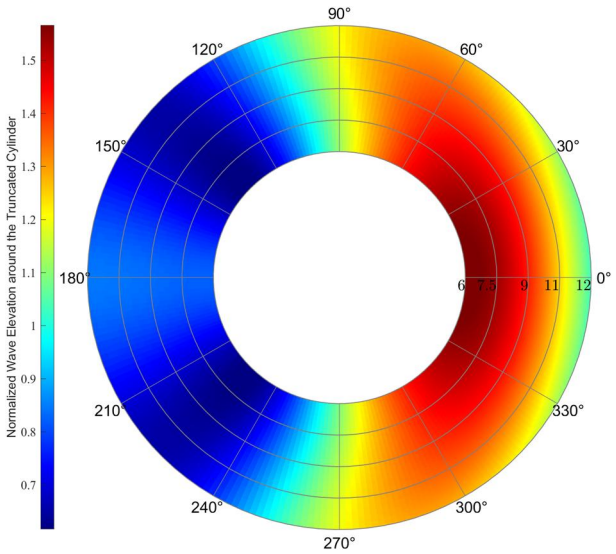

(b)

Figure 4.7 Distribution of wave amplitude around the truncated cylinder with porous dual damping plate ($b_0 = 23, b_1/h = 0.025$) with different scattering parameters: (a) ka=0.2; (b) ka=1

Fig 4.6 and Fig 4.7 illustrate the distribution of wave amplitude around the truncated cylinder with dual damping plates under different porosities. It is evident that when the wavelength of the incident wave is very long (*ka*=0.2), the wave elevations on the lee side and the weather side of the truncated cylinder are almost symmetrical. Additionally, there is a consistent decreasing tendency of wave run-up on the surface of the truncated cylinder from the front point (0°) to the rear point (90°). When the wavelength becomes very long (*ka*=1), the magnitude of water level on the weather side of the truncated cylinder is much higher than that on the lee side. In this case, wave run-up gradually decreases from the front point (0°) to the back shoulder point (135°) of the truncated cylinder. Ultimately, it can be concluded that the upper damping plate with greater porosity could effectively reduce wave run-up around the truncated cylinder.

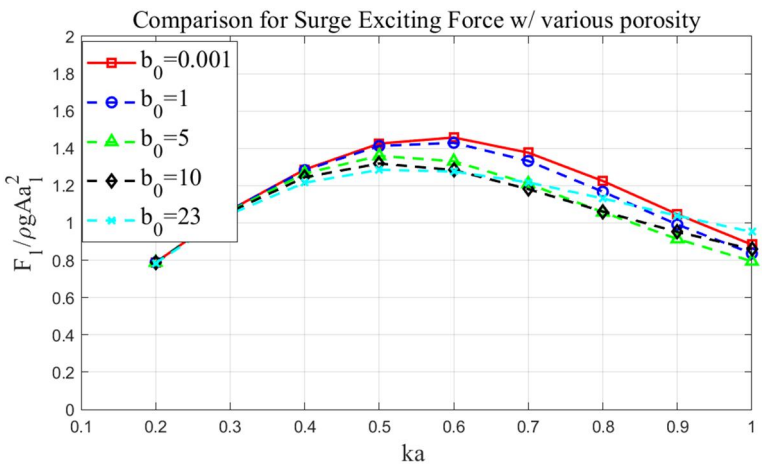

(a)

Figure 4.8 (Continued)

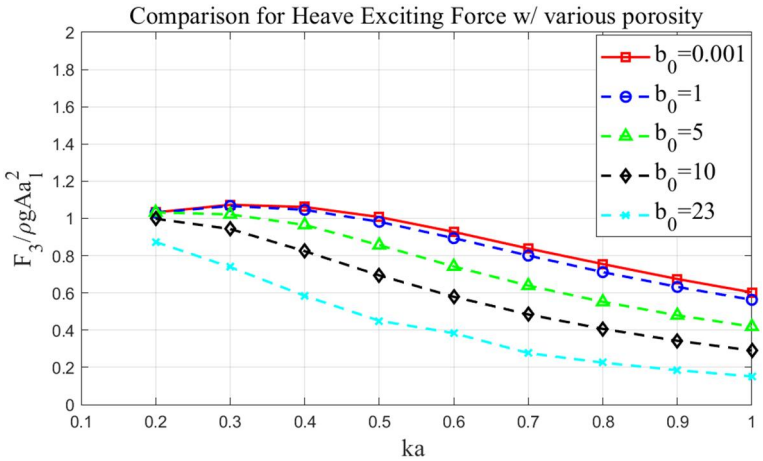

(b)

Figure 4.8 Comparison of wave exciting forces around the truncated cylinder with different b_0 for upper damper ($b_1/h = 0.025$): (a) surge exciting force; (b) heave exciting force

Regarding the porous damping plate, the hydrodynamic forces acting on the truncated cylinder have been investigated. Fig. 4.8 shows the variation of surge and heave wave exciting forces versus the scattering parameter *ka* for different porous effect parameter (b_0) of the upper damping plate. The heave wave exciting force acting on the truncated cylinder decreases significantly due to the larger porosity of the upper damping plate, whereas the surge wave exciting force does not show significant change. As noted, in present MEEM solution, the thicknesses of the dual damping plate are zero, resulting in a very small changes on surge wave exciting force. However, with regard to the heave wave exciting force, the pressure gap between the two sides of the upper damping plate also varies substantially as the porosity changes. Thus, the heave wave exciting force acting on upper damping plate is quite sensitive to its porosity. Compared to short wave cases, the hydrodynamic loads on the truncated

cylinder under long wave conditions are not significantly affected by the porosity, which is in line with the behavior of wave run-up.

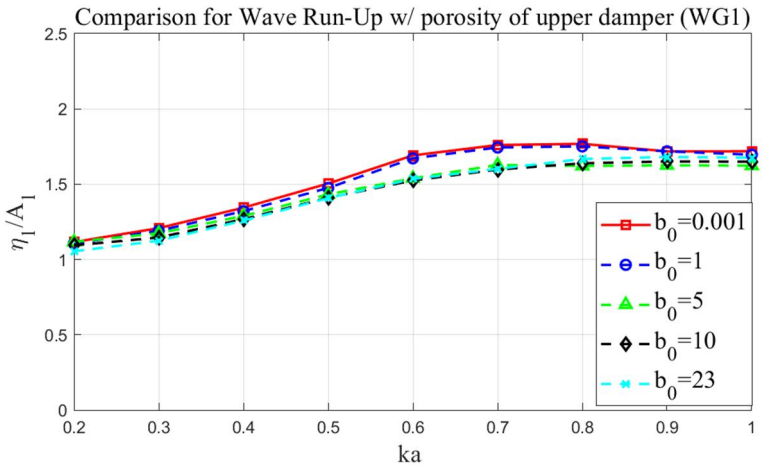

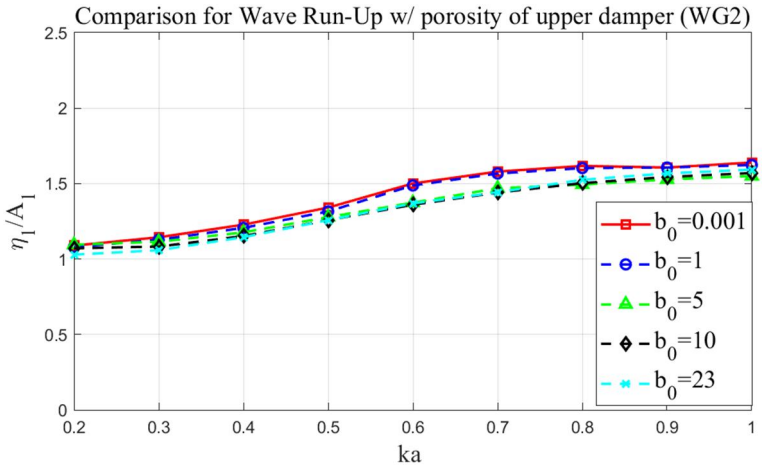

Figure 4.9 (Continued)

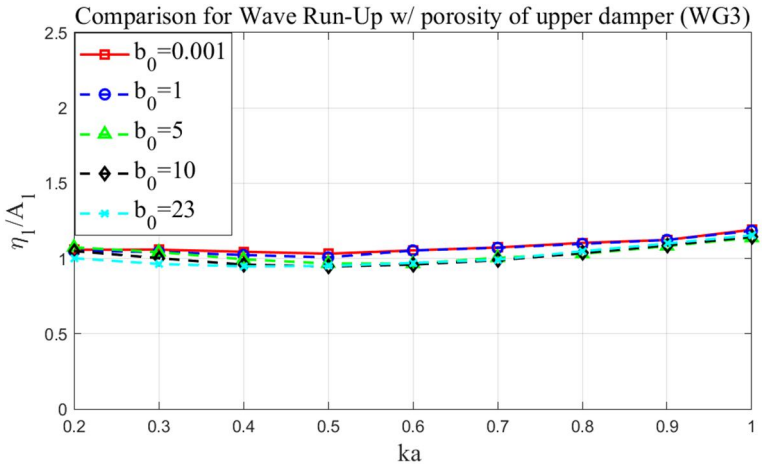
Comparison for Wave Run-Up w/ porosity of upper damper (WG3)
b0=0.001
b0=1
b0=5
b0=10
b0=23
η1/A1
ka
0
0.5
1
1.5
2
2.5
0.2
0.3
0.4
0.5
0.6
0.7
0.8
0.9
1

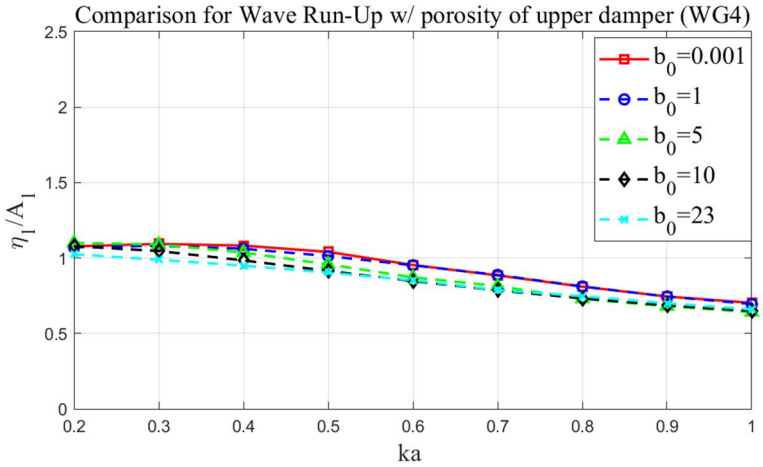
Comparison for Wave Run-Up w/ porosity of upper damper (WG4)
b0=0.001
b0=1
b0=5
b0=10
b0=23
η1/A1
ka
0
0.5
1
1.5
2
2.5
0.2
0.3
0.4
0.5
0.6
0.7
0.8
0.9
1

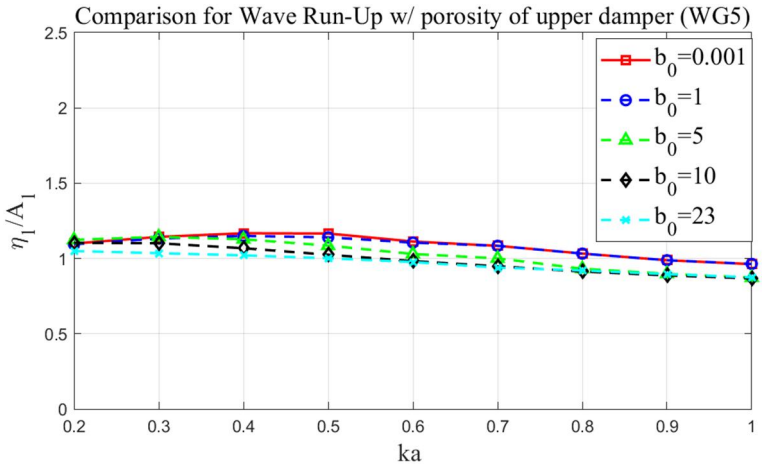
Comparison for Wave Run-Up w/ porosity of upper damper (WG5)
b0=0.001
b0=1
b0=5
b0=10
b0=23
η1/A1
ka
0
0.5
1
1.5
2
2.5
0.2
0.3
0.4
0.5
0.6
0.7
0.8
0.9
1

Figure 4.9 Comparison of wave run-up around the truncated cylinder with different b_0 for upper damper ($b_1/h = 0.05$)

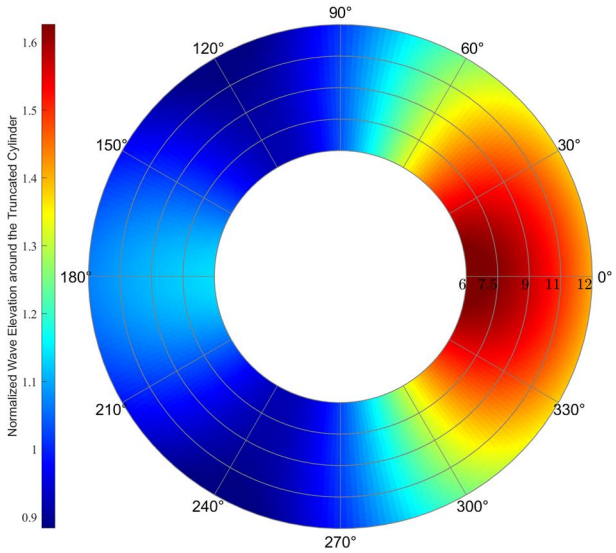

(a)

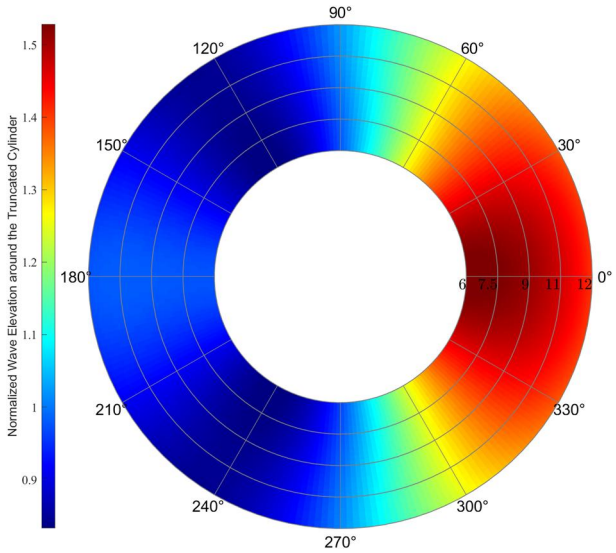

(b)

Figure 4.10 Distribution of wave amplitude around the truncated cylinder

with porous dual damping plate ($ka = 0.6, b_1/h = 0.05$) with various porosities: (a) b_0=0.001; (b) b_0=23

Fig. 4.9 shows the effect of porosity of the upper damping plate on the wave elevations around the truncated cylinder for $ka = 0.6, b_1/h = 0.05$. The position of the upper damping plate moves downward ($b_1/h = 0.05$) relative to the case in Fig. 4.5. Compared with large separating distance ($b_1/h = 0.025$), the decreasing effect on wave run-up due to the porosity becomes weaker under small separating distance. The phenomenon of wave elevation distribution with respect to the small separating distance ($b_1/h = 0.05$) is demonstrated in Fig.4.10. When $ka = 0.6$, the local water level adjacent to the truncated cylinder is not strongly affected by the porosity of upper damping plate. It can therefore be concluded that the attenuating effect due to the porous upper damping plate is quite strong when the upper damping plate is close to the still water level. While the influences become very weak when the position of the upper damping plate is relatively low.

4.3 Effect of thickness

In the real engineering problem, it is impossible to neglect the thickness of the heave damping plate. In this section, the effect of thickness for the single damping plate on wave run-up is investigated. To apply the present MEEM solution to the truncated cylinder with thick damping plate, an additional matching condition (Eq. 4.1) for the velocity potential in exterior region is needed except for the previous matching conditions (Eq. 2.6).

$$\frac{\partial \phi_3}{\partial r} = 0 \qquad \text{for} \quad -b_1 \geq z \geq -b_2,\ r = a_2 \tag{4.1}$$

Regarding the truncated cylinder with thick damping plate, the horizontal velocity of the fluid in exterior region becomes zero on the surface of thick damping plate. The geometric parameters are set to $a_1/a_2 = 0.5, a_2/h = 0.06, b_2/h = 0.1, b_0 = 0.001$ without the consideration of porous effect. Fig. 4.11 shows the variation of wave run-up around the truncated cylinder versus the scattering parameter (*ka*) for various normalized thickness (T/D). Here *T* represents the thickness of single damping plate and *D* is the draft of the truncated cylinder.

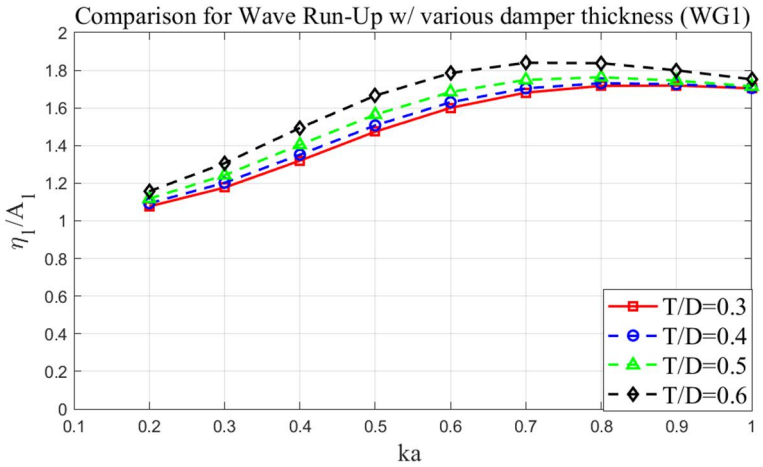
Comparison for Wave Run-Up w/ various damper thickness (WG1)
η_1/A_1
ka
T/D=0.3
T/D=0.4
T/D=0.5
T/D=0.6

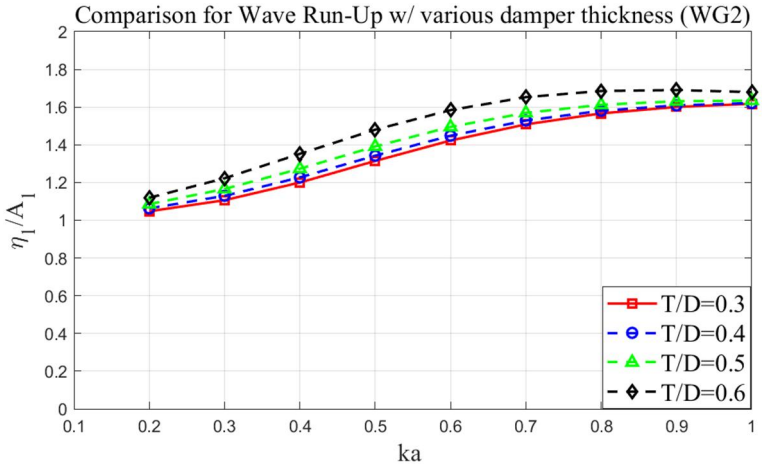
Comparison for Wave Run-Up w/ various damper thickness (WG2)
η_1/A_1
ka
T/D=0.3
T/D=0.4
T/D=0.5
T/D=0.6

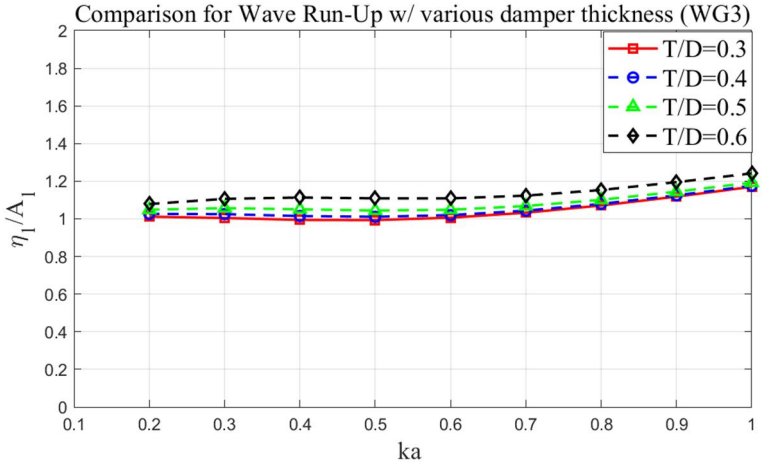
Comparison for Wave Run-Up w/ various damper thickness (WG3)
η_1/A_1
ka
T/D=0.3
T/D=0.4
T/D=0.5
T/D=0.6

Figure 4.11 (Continued)

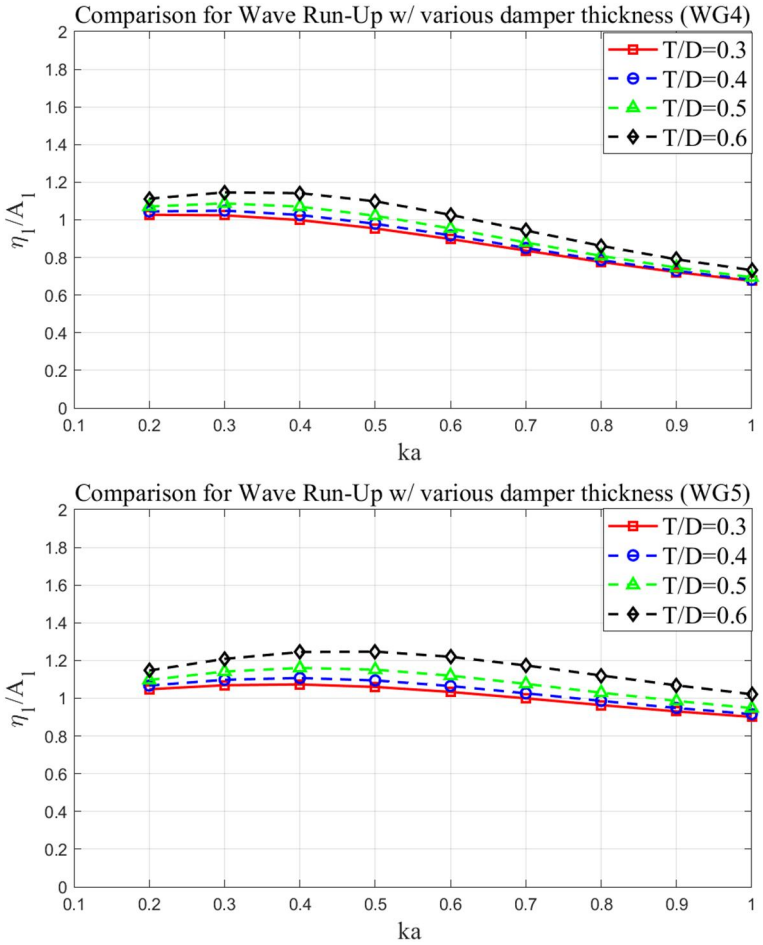

Figure 4.11 Comparison of wave run-up around the truncated cylinder with different normalized thickness T/D of single thick damper

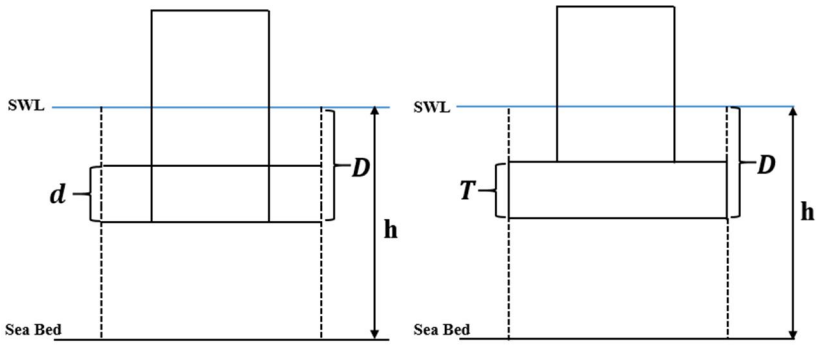

Figure 4.12 Schematic of truncated cylinder with single thick damper and dual thin damping plates

As the thickness of single damping plates increases, the wave elevations on both the lee side and the weather side of truncated cylinder increase, which is in line with the behaviors of dual damping plate. Additionally, under different diffraction parameters conditions, as the single damping plate becomes thicker, the wave elevations increase more significantly. It implies that as the top surface of the thick damper gets close to the free surface, the enhancement of wave run-up around the truncated cylinder becomes more substantial. The schematic of cylinders with the dual thin damping plates and the single thick damper are shown in Fig. 4.12. The major difference between two cylinder models is that in the case of the cylinder with the dual thin damping plates, there is no sidewall on the edge of dual damping plates compared to the cylinder with the single thick damper. To investigate the effect of the sidewall of the damping plate, wave run-up comparison results are demonstrated in Fig.4.13. Here, the separating distance (d/D) between dual damping plates is set to be identical to the thickness (T/D) of the single damping plate. Overall, the increment of wave run up looks similar between two cylinder models. On the weather side, wave run-up is almost similar between the single thick damper and the dual thin

dapmers. On the lee side of the truncated cylinder with the single thick damper, the local water level is slightly higher than dual damping plates. Which implies that the sidewall of the thick damping plate can not affect the wave elevation significantly.

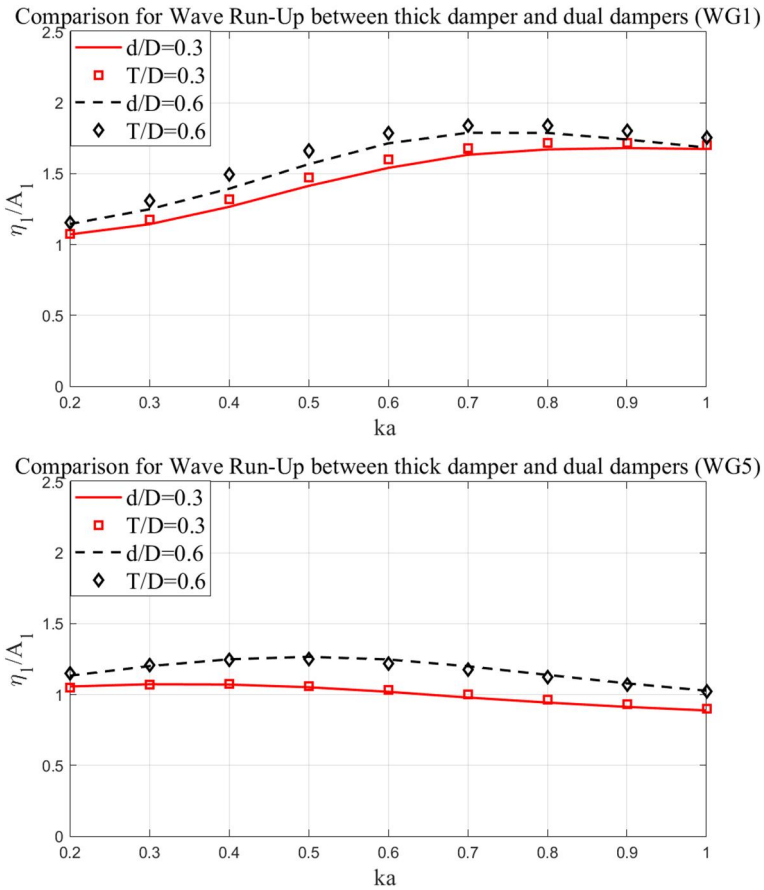

Figure 4.13 Comparison of wave run-up around truncated cylinder with dual damping plate and single thick damper

5. Conclusions

This study aims to investigate the diffraction problem for a fixed truncated cylinder with porous dual damping plates. To solve this problem, an analytical solution based on the matched eigen-function expansion method (MEEM) was developed. Two series of validation approaches were proposed: wave diffraction for truncated cylinders with various impermeable damping plates and wave diffraction for simple porous structures. The numerical validation for wave run-up around the truncated cylinder with various impermeable damping plates was conducted by comparing with BEM solutions, which yielded good agreement. Furthermore, the complex wave number and hydrodynamic loads on simple porous structures such as horizontal porous membrane were also validated by comparing with previous computational results.

In this study, three different types of heave damping plates were applied to the truncated cylinder: a single thin damping plate, a single thick damping plate and dual thin damping plates. The numerical results of the truncated cylinder with porous dual damping plates showed that wave run-up as well as heave wave exciting force acting on the truncated cylinder could be significantly reduced by applying the porous upper damping plate. However, the surge wave exciting force was not sensitive to the porosity of the upper damper. Regarding the cylinder with impermeable dual damping plates, the heave exciting force and wave elevations around the cylinder increased due to the shallow water effect in the local flow as the separating distance increased. It was also confirmed that the thickness of the damping plate could affect the wave-body interaction for the truncated cylinder. As the damper became thicker, an increment of wave run-up was clearly observed, though the influence was not as dramatic as the porosity. In conclusion, it has been confirmed that more

favorable wave run-up and hydrodynamic performance of the truncated cylinder could be obtained by using porous dual damping plates. This type of damper is expected to be applied to offshore structures such as FOWT.

In the future, model tests will be conducted to validate the analytical solution. In addition to the diffraction problem, present MEEM model will also be extended to solve the radiation problem for the truncated cylinder with dual damping plates with the consideration of porosity. Furthermore, the effect of porous damping plate on added mass, damping forces acting on the cylinder will be investigated.

Reference

[1] Walter Musial, Paul Spitsen, Philipp Beiter, Partick Duffy, Melinda Marquis, Aubryn Cooperman, Rob Hammond, Matt Shields (2021) Offshore Wind Market Report: 2021 Edition.

[2] InfoLink. (2021) Floating wind turbine II: Floating structure technology and market trends. https://www.infolink-group.com/energy-article/Floating-wind-turbine-II-Floating-structure-technology-and-market-trends (accessed DEC.17,2021)

[3] Roddier, D., Cermelli, C., Aubault, A., & Weinstein, A. (2010). WindFloat: A floating foundation for offshore wind turbines. Journal of renewable and sustainable energy, 2(3), 033104.

[4] Robertson, A., Jonkman, J., Masciola, M., Song, H., Goupee, A., Coulling, A., & Luan, C. (2014). Definition of the semisubmersible floating system for phase II of OC4 (No. NREL/TP-5000-60601). National Renewable Energy Lab.(NREL), Golden, CO (United States).

[5] Lefebvre, S., & Collu, M. (2012). Preliminary design of a floating support structure for a 5 MW offshore wind turbine. Ocean engineering, 40, 15-26.

[6] Huijs, F., de Bruijn, R., & Savenije, F. (2014). Concept design verification of a semi-submersible floating wind turbine using coupled simulations. Energy Procedia, 53, 2-12.

[7] Europe, W. (2018). Floating offshore wind energy: a policy blueprint for Europe. Position Paper, 10.

[8] Mohapatra, Sarat Chandra, Hafizul Islam, and C. Guedes Soares (2020). "Boussinesq model and CFD simulations of non-linear wave diffraction by a floating vertical cylinder." Journal of Marine Science and Engineering 8.8: 575.

[9] Mohseni, Mohammad, Paulo T. Esperanca, and Sergio H. Sphaier (2018). "Numerical study of wave run-up on a fixed and vertical surface-piercing cylinder subjected to regular, non-breaking waves using OpenFOAM." Applied Ocean Research 79: 228-252.

[10] Morris-Thomas, M. T., and K. P. Thiagarajan (2004). "The run-up on a cylinder in progressive surface gravity waves: harmonic components." Applied Ocean Research 26.3-4: 98-113.

[11] Lee, Jong-Hyun, and Bonguk Koo (2021). "Numerical Study of Non-Linear Wave run-up Around a Circular Cylinder in Regular Waves." Journal of Coastal Research 114.SI: 554-558.

[12] Cha, Kyung-Jung, et al. "Numerical study of wave run-up around offshore structure in waves." Journal of Advanced Research in Ocean Engineering 2.2 (2016): 61-66.

[13] Cao, H. J., & Wan, D. C. (2015). RANS-VOF solver for solitary wave run-up on a circular cylinder. China Ocean Engineering, 29(2), 183-196.

[14] Nam, B. W., Sung, H. G., Kim, Y. S., & Hong, S. Y. (2008). Experiments second-order computations for run-up around a truncated cylinder in waves. Journal of Ships & Ocean Engineering, 46, 43-52.

[15] Kim, J., Jaiman, R., Cosgrove, S., & O'Sullivan, J. (2011). Numerical wave tank analysis of wave run-up on a truncated vertical cylinder. In International Conference on Offshore Mechanics and Arctic Engineering (Vol. 44335, pp. 805-814).

[16] Bao, W., Zhao, F., & Kinoshita, T. (2009, January). Calculation of wave forces acting on a cylinder with a porous plate fixed inside. In International Conference on Offshore Mechanics and Arctic Engineering (Vol. 43444, pp. 1253-1260).

[17] Chwang, A. T., & Wu, J. (1994). Wave scattering by submerged porous disk. Journal of engineering mechanics, 120(12), 2575-2587.

[18] Tao, L., Lim, K. Y., & Thiagarajan, K. (2004). Heave response of classic spar with variable geometry. J. Offshore Mech. Arct. Eng., 126(1), 90-95.

[19] Sudhakar, S., & Nallayarasu, S. (2011, January). Influence of heave plate on hydrodynamic response of spar. In International Conference on Offshore Mechanics and Arctic Engineering (Vol. 44335, pp. 437-447).

[20] Subbulakshmi, A., & Sundaravadivelu, R. (2016). Heave damping of spar platform for offshore wind turbine with heave plate. Ocean Engineering, 121, 24-36.

[21] Rao, M. J., Nallayarasu, S., & Bhattacharyya, S. K. (2021). CFD approach to heave damping of spar with heave plates with experimental validation. Applied Ocean Research, 108, 102517.

[22] Thiagarajan, K. P., Datta, I., Ran, A. Z., Tao, L., & Halkyard, J. E. (2002, January). Influence of heave plate geometry on the heave response of classic spars. In International Conference on Offshore Mechanics and Arctic Engineering (Vol. 36118, pp. 621-627).

[23] Zhao, F. F., Kinoshita, T., Bao, W. G., Huang, L. Y., Liang, Z. L., & Wan, R. (2012). Interaction between waves and an array of floating porous circular cylinders. China Ocean Engineering, 26(3), 397-412.

[24] Williams, A. N., & Li, W. (2000). Water wave interaction with an array of bottom-mounted surface-piercing porous cylinders. Ocean Engineering, 27(8), 841-866.

[25] Li, Y., Sun, L., & Teng, B. (2004, September). Wave interaction with an array of combined cylinders with solid interior column and porous exterior column. In The Sixth ISOPE Pacific/Asia Offshore Mechanics Symposium. OnePetro.

[26] Sankarbabu, K., Sannasiraj, S. A., & Sundar, V. (2007). Interaction of regular waves with a group of dual porous circular cylinders. Applied Ocean Research, 29(4), 180-190.

[27] Park, M. S., Jeong, Y. J., You, Y. J., & Kim, H. C. (2014). Numerical analysis of a gravity substructure with partial porous area for offshore wind turbines. Journal of Civil Engineering and Architecture Research, 1(4), 230-238.

[28] Feichtner, A., Mackay, E., Tabor, G., Thies, P. R., Johanning, L., & Ning, D. (2021). Using a porous-media approach for CFD modelling of wave interaction with thin perforated structures. Journal of Ocean Engineering and Marine Energy, 7(1), 1-23.

[29] George, A., & Cho, I. H. (2022). Numerical and experimental assessment of hydrodynamic force of a heaving porous disk. Ships and Offshore Structures, 1-10.

[30] Mackay, E., Liang, H., & Johanning, L. (2021). A BEM model for wave forces on structures with thin porous elements. Journal of Fluids and Structures, 102, 103246.

[31] Havelock, T. H. (1940). The pressure of water waves upon a fixed obstacle. Proceedings of the Royal Society of London. Series A. Mathematical and Physical Sciences, 175(963), 409-421.

[32] Omer Jr, G. C., & Hall, H. H. (1949). The scattering of a tsunami by a cylindrical island. Bulletin of the Seismological Society of America, 39(4), 257-260.

[33] MacCamy, R. C., & Fuchs, R. A. (1954). Wave forces on piles: a diffraction theory (No. 69). US Beach Erosion Board.

[34] Cho, I. H., & Kim, M. H. (2000). Interactions of horizontal porous flexible membrane with waves. Journal of waterway, port, coastal, and ocean engineering, 126(5), 245-253.

[35] Yu, X. (1995). Diffraction of water waves by porous breakwaters. Journal of waterway, port, coastal, and ocean engineering, 121(6), 275-282.

[36] Zhao, F., Bao, W., Kinoshita, T., & Itakura, H. (2011). Theoretical and experimental study on a porous cylinder floating in waves. Journal of offshore mechanics and Arctic engineering, 133(1).

[37] Mandal, S., N. Datta, and T. Sahoo. "Hydroelastic analysis of surface wave interaction with concentric porous and flexible cylinder systems." Journal of Fluids and Structures 42 (2013): 437-455.

[38] Liu, Y., Li, Y. C., & Teng, B. (2007). Wave interaction with a perforated wall breakwater with a submerged horizontal porous plate. Ocean Engineering, 34(17-18), 2364-2373.

[39] Ning, D. Z., Zhao, X. L., Teng, B., & Johanning, L. (2017). Wave diffraction from a truncated cylinder with an upper porous sidewall and an inner column. Ocean Engineering, 130, 471-481.

[40] Sarkar, A., & Bora, S. N. (2020). Hydrodynamic forces and moments due to interaction of linear water waves with truncated partial-porous cylinders in finite depth. Journal of Fluids and Structures, 94, 102898.

[41] Wang, G., Yu, F., Zhang, H., Zhang, E., & Li, Z. (2021). Wave diffraction from a concentric truncated cylinder system with a porous ring plate fixed inside. Ocean Engineering, 228, 108932.

[42] Park, M. S., & Koo, W. (2015). Mathematical modeling of partial-porous circular cylinders with water waves. Mathematical Problems in Engineering, 2015.

[43] Yeung, R. W. (1981). Added mass and damping of a vertical cylinder in finite-depth waters. Applied Ocean Research, 3(3), 119-133.

[44] Bhatta, D. D., & Rahman, M. (2003). On scattering and radiation problem for a cylinder in water of finite depth. International Journal of Engineering Science, 41(9), 931-967.

[45] Finnegan, W., Meere, M., & Goggins, J. (2013). The wave excitation forces on a truncated vertical cylinder in water of infinite depth. Journal of Fluids and Structures, 40, 201-213.

[46] Linton, C. M., & McIver, P. (2001). Mathematical techniques for wave/structure interactions.

[47] Atkinson, F. V. (1949). LXI. On Sommerfeld's “radiation condition.”. The London, Edinburgh, and Dublin Philosophical Magazine and Journal of Science, 40(305), 645-651.

[48] Zienkiewicz, O. C., Kelly, D. W., & Bettess, P. (1979). The Sommerfeld (radiation) condition on infinite domains and its modelling in numerical procedures. In Computing Methods in Applied Sciences and Engineering, 1977, I (pp. 169-203). Springer, Berlin, Heidelberg.

[49] Chwang, A. T. (1983). A porous-wavemaker theory. Journal of Fluid Mechanics, 132, 395-406.

[50] Taylor, G. I. (1956). Fluid flow in regions bounded by porous surfaces. Proceedings of the Royal Society of London. Series A. Mathematical and Physical Sciences, 234(1199), 456-475.

[51] A Muheadden, S. (2010). A New Technique to Compute Complex Roots. Kirkuk University Journal-Scientific Studies, 5(1), 104-113.

[52] Liu, P. L. (1973). Damping of water waves over porous bed. Journal of the Hydraulics Division, 99(12), 2263-2271.

[53] McIver, P. (1998). The dispersion relation and eigenfunction expansions for water waves in a porous structure. Journal of engineering mathematics, 34(3), 319-334.

[54] Mendez, F. J., & Losada, I. J. (2004). A perturbation method to solve dispersion equations for water waves over dissipative media. Coastal engineering, 51(1), 81-89.

[55] Craik, A. D. (1988). Wave interactions and fluid flows. Cambridge University Press.

[56] Dalrymple, R. A., Losada, M. A., & Martin, P. A. (1991). Reflection and transmission from porous structures under oblique wave attack. Journal of fluid mechanics, 224, 625-644.

[57] Yu, X., & Chwang, A. T. (1993). Analysis of wave scattering by submerged circular disk. Journal of engineering mechanics, 119(9), 1804-1817.

[58] Siemens, P. (2018). Simcenter STAR-CCM+ user guide V13. 04. Siemens PLM.

[59] Perić, R., & Abdel-Maksoud, M. (2018). Analytical prediction of reflection coefficients for wave absorbing layers in flow simulations of regular free-surface waves. Ocean Engineering, 147, 132-147.

[60] Peric, R. (2019). Minimizing undesired wave reflection at the domain boundaries in flow simulations with forcing zones. Technische Universität Hamburg.

[61] Kim, M. W., Koo, W., & Hong, S. Y. (2014). Numerical analysis of various artificial damping schemes in a three-dimensional numerical wave tank. Ocean engineering, 75, 165-173.